Hippocampus Modulates Natural Sound Processing at Early Auditory Centers

Eddie C. Wong[1,2], Xunda Wang[1,2], Ed X. Wu[1,2,3*], Alex T. L. Leong[1,2*]

[1]Laboratory of Biomedical Imaging and Signal Processing, The University of Hong Kong, Pokfulam, Hong Kong SAR, China
[2]Department of Electrical and Electronic Engineering, The University of Hong Kong, Pokfulam, Hong Kong SAR, China
[3]School of Biomedical Sciences, LKS Faculty of Medicine, The University of Hong Kong, Pokfulam, Hong Kong SAR, China

[*]Correspondence should be addressed to Ed X. Wu, Ph.D. and Alex T. L. Leong, Ph.D.:
Laboratory of Biomedical Imaging and Signal Processing, Department of Electrical and Electronic Engineering, The University of Hong Kong, Pokfulam, Hong Kong, Hong Kong SAR, China.
Fax: +852-2859-8738.
Tel: +852-2859-7096.
Email: ewu@eee.hku.hk & tlleong@eee.hku.hk

Keywords

fMRI; Auditory system; Hippocampus; Inferior colliculus; Medial geniculate body; Auditory cortex; Optogenetics; Vocalizations

Author Contributions

E.C.W., A.T.L.L., and E.X.W. designed research; E.C.W. performed research; E.C.W., X.W., A.T.L.L., and E.X.W. analyzed data; X.W. provided technical assistance; and E.C.W., A.T.L.L., and E.X.W. wrote the paper.

Abstract

Despite its prominence in learning and memory, hippocampal influence in early auditory processing centers remains unknown. Here, we examined how hippocampal activity modulates sound-evoked responses in the auditory midbrain and thalamus using optogenetics and functional MRI (fMRI) in rodents. Ventral hippocampus (vHP) excitatory neuron stimulation at 5 Hz evoked robust hippocampal activity that propagates to the primary auditory cortex. We then tested 5Hz vHP stimulation paired with either natural vocalizations or artificial/noise acoustic stimuli. vHP stimulation enhanced auditory responses to vocalizations (with a negative or positive valence) in the inferior colliculus, medial geniculate body, and auditory cortex, but not to their temporally reversed counterparts (artificial sounds) or broadband noise. Meanwhile, pharmacological vHP inactivation diminished response selectivity to vocalizations. These results directly reveal the large-scale hippocampal participation in natural sound processing at early centers of the ascending auditory pathway. They expand our present understanding of hippocampus in global auditory networks.

Introduction

In the central auditory system, auditory input from the ear transmits to the inferior colliculus (IC), medial geniculate body (MGB) in thalamus, and auditory cortex (AC) along the ascending auditory pathway (1-3). Information is hierarchically relayed along this ascending pathway, as distinct auditory features like amplitude and frequency are gradually extracted and processed throughout each auditory center (3-7). Existing functional frameworks describing auditory processing in the ascending auditory pathway are often examined using basic stimuli such as pure tones and broadband noise (8-10). However, neural representation of simplified acoustic stimuli may not reliably predict responses to natural sounds (8, 11-13), such as vocalizations, which are critical for facilitating communications and behavioral responses (14-16). Natural sound processing requires decoding complex spectrotemporal dynamic properties (17, 18) and additional input from higher-order regions is needed to facilitate tacitly assumed auditory functions such as communication, learning, and memory processes (19-22). Despite the current consensus on the pivotal roles played by AC corticofugal projections in natural sound processing (7, 23-25), emerging structural evidence has revealed that auditory midbrain and thalamus project to non-auditory regions such as superior colliculus (26) and striatum (27), respectively, and receive afferents from sensory, prefrontal, and limbic regions (28, 29). These findings suggest that information can transmit in and out of early auditory centers in the ascending pathway to cortex and beyond, parallel with those at the AC level in the processing hierarchy. We speculate that the auditory network for natural sound processing is far more brain-wide than presently known.

Given its roles in memory, emotion, and learning functions (30-32), we contend that the hippocampus is a strong candidate to participate in brain-wide auditory processing of natural sounds. Notably, the hippocampus has been indirectly linked with auditory processing (33, 34).

Functional studies indicate interactions between the hippocampus and auditory cortex during learning and memory processes. Electrophysiology studies demonstrate that the hippocampus actively engages the auditory cortex to transform auditory inputs into long-term memories that are subsequently consolidated in cortical networks (35, 36). Meanwhile, studies show that specific hippocampal neurons only respond to sounds associated with a trained sound behavioral task (22, 36), implying that the hippocampus participates in the interpretation of complex auditory inputs. Anatomically, the hippocampus can receive and relay auditory signals via reciprocal projections directly with AC (37, 38) and indirectly through parahippocampal regions (38, 39) and forebrain pathways (19, 40), such as the entorhinal cortex, amygdala and medial septum complex. Tracing studies also indicated indirect projections, albeit scarcer, from the hippocampus to the IC and MGB via parahippocampal regions and amygdala (28, 29, 41). However, existing studies have not directly examined the role of the hippocampus in processing auditory inputs at these early auditory centers. Further, most studies so far focus on the cortex. They provide little to no evidence of the possible functional interactions between the hippocampus and auditory regions at the midbrain and thalamic levels. At present, whether and how the hippocampus functionally influences auditory responses, especially in the early ascending auditory centers, remains unknown.

Here, we posit that the hippocampus participates in natural sound processing at early sound processing centers within the ascending auditory pathway, especially the IC and MGB. The ventral hippocampus (vHP) plays a role in processing sensory inputs with an emotional context (42, 43), thus it may influence natural sound processing throughout the ascending pathway. In this study, we examined whether optogenetically evoked vHP activity modulates sound processing in the auditory midbrain, thalamus and cortex. Using a combined optogenetic cell-specific stimulation of Ca^{2+}/calmodulin-dependent protein kinase IIα (CaMKIIα)-expressing vHP neurons and whole-

brain functional MRI (fMRI) visualization, we assessed blood-oxygenation-level dependent (BOLD) fMRI responses to two different categories of sound – natural sound (i.e., vocalizations) and artificial/basic acoustic stimuli. We revealed that the vHP activity enhances auditory responses to vocalizations, but not artificial stimuli or noise, in the IC, MGB and AC.

Results

Brain-wide propagation of neural activity initiated at ventral hippocampus

We characterized the downstream targets of the ventral hippocampus (vHP) using optogenetics to selectively stimulate CaMKIIα-expressing vHP excitatory neurons, primarily in the dentate gyrus of vHP. Anatomical MRI scans confirmed the location of the virus injection and optical fiber implantation in vHP of all animals (**Figure 1A**). Immunohistochemistry confirmed that CaMKIIα$^+$ excitatory neurons of the vHP (**Figure 1B**), but not GABAergic inhibitory neurons, expressed ChR2-mCherry (**Supplementary Figure 1A**).

To examine frequency-dependent spatiotemporal characteristics of brain-wide, long-range evoked BOLD responses driven by vHP, we performed whole-brain optogenetic fMRI in lightly anesthetized rats. Blue light pulses at five frequencies (1 Hz with 10 % duty cycle, 5 Hz, 10 Hz, 20 Hz, and 40 Hz with 30 % duty cycle; light intensity, 40 mW/mm^2) were delivered to vHP neurons in a block design paradigm (**Supplementary Figure 2A**). We chose a reduced duty cycle for 1 Hz stimulation to avoid excessively long stimulation pulse width that may not be physiological. 5 Hz optogenetic stimulation of vHP evoked robust brain-wide positive BOLD activations in regions related to learning, memory, sensory processing and emotion, including bilateral vHP, dorsal hippocampus (dHP), entorhinal cortex (Ent), primary auditory cortex (AC),

perirhinal cortex (Prh), amygdala (AMG), medial septum (MS), lateral septum (LS), diagonal band of Broca (DBB), and cingulate cortex (Cg) (**Figure 2**). Note that we did not detect any positive BOLD activations in IC and MGB in midbrain and thalamus, respectively. Such brain-wide activations evoked by 5 Hz stimulation indicated a high possibility of sound processing modulation. Further, this frequency matches the previously reported range of hippocampal theta oscillations, which travels along the hippocampal septotemporal axis (44, 45). Importantly, we found robust BOLD activations in the AC only during 5 Hz stimulation at vHP, but not at the other four frequencies (1 Hz, 10 Hz, 20 Hz, 40 Hz) (**Supplementary Figure 2C**). These frequencies evoked weaker BOLD responses in Prh, MS, and LS, and Cg, while retaining strong BOLD responses in vHP and dHP. Altogether, these results demonstrate the most extensive brain-wide vHP downstream targets found at 5 Hz stimulation, especially the robust BOLD activations in AC. These findings indicate that 5 Hz vHP stimulation generates strong and robust hippocampal activity outputs to AC and other regions, likely modulating sound processing brain-wide.

Hippocampal outputs enhance neural responses and their selectivity to vocalizations with negative valence in auditory midbrain, thalamus and cortex

To explore the large-scale hippocampal modulatory effects on early auditory processing of natural sound, we performed auditory fMRI with and without continuous 5 Hz optogenetic stimulation at vHP. Forward aversive vocalizations (i.e., natural and behaviorally relevant) and the same but temporally reversed vocalizations (i.e., artificial and behaviorally irrelevant) were presented to the contralateral/left ear in a block-design paradigm (**Supplementary Figure 3A**). As expected, auditory evoked BOLD responses occurred along the ascending auditory pathway, including ipsilateral IC, MGB, and bilateral AC (**Figure 3**). Without optogenetic stimulation, the BOLD responses (as described by β values) in IC, MGB and AC were stronger using forward than

reversed vocalizations (with β percentage difference between forward and reversed vocalization responses in IC: 8.6 ± 2.7 %, $p < 0.01$; MGB: 34.7 ± 10.53 %, $p < 0.05$; AC: 22.0 ± 7.7 %, $p < 0.05$, paired Student's t-test followed by Holm-Bonferroni correction). This finding demonstrates the response selectivity to forward vocalizations, which is consistent with our prior findings in rodent auditory system (46). Here, the response selectivity was most prominent in the external cortex (ECIC) and dorsal cortex (DCIC) of IC (with β percentage difference in ECIC: 8.8 ± 2.6 %, $p < 0.01$; DCIC: 7.8 ± 1.6 %, $p < 0.01$, paired Student's t-test followed by Holm-Bonferroni correction).

Optogenetic 5 Hz vHP stimulation significantly enhanced response selectivity to forward vocalizations throughout the ascending auditory pathway (with the β percentage difference between forward and reversed vocalization responses in IC: 16.3 ± 3.5 %, $p < 0.01$; MGB: 166.2 ± 57.6 %, $p < 0.01$; AC: 46.5 ± 11.9 %, $p < 0.001$, paired Student's t-test followed by Holm-Bonferroni correction). Specifically, only the BOLD responses in IC, MGB and AC evoked by the forward vocalizations were significantly increased by optogenetic stimulation (with β percentage increase in forward vocalization response in IC: 18.2 ± 7.3 %, $p < 0.05$; MGB: 76.5 ± 22.6 %, $p < 0.01$; AC: 28.7 ± 14.1 %, $p < 0.05$, paired Student's t-test followed by Holm-Bonferroni correction). This finding demonstrates that the hippocampal outputs selectively modulate the responses to forward vocalizations that convey contextual information. Note that such increased responses in IC occurred in ECIC and DCIC, as well as CNIC (with β increase in ECIC: 20.5 ± 9.5%, $p < 0.05$; DCIC: 20.8 ± 4.2 %, $p < 0.001$, CNIC: 26.3 ± 6.1 %, $p < 0.01$, paired Student's t-test followed by Holm-Bonferroni correction). Altogether our fMRI results indicate that hippocampal outputs (initiated by the 5 Hz vHP stimulation) can enhance IC, MGB and AC auditory responses and their

155 selectivity to natural and behaviorally relevant sounds at early processing centers within the
156 ascending auditory pathway.

157 **Hippocampal outputs enhance neural responses and their selectivity to vocalizations with**
158 **positive valence**

159 We then utilized the same approach to examine whether such hippocampal modulation on
160 natural sound processing was biased for only the aversive content in vocalizations. So, we
161 performed auditory fMRI with postejaculatory vocalizations with and without presenting the 5 Hz
162 optogenetic stimulation at vHP. Similarly, auditory evoked BOLD responses occurred along the
163 ascending auditory pathway, including IC, MGB, and AC (**Figure 4**). Without optogenetic
164 stimulation, the BOLD responses evoked by postejaculatory vocalizations also showed response
165 selectivity to the forward one (with β percentage difference between forward and reversed
166 vocalization responses in IC: 7.8 ± 1.7 %, $p < 0.001$; MGB: 43.0 ± 16.2 %, $p < 0.05$; AC: 40.5 ±
167 14.4 %, $p < 0.05$, paired Student's t-test followed by Holm-Bonferroni correction). Consistent with
168 the results of aversive vocalization experiment, the response selectivity to forward postejaculatory
169 vocalizations in IC was mainly observed in ECIC and DCIC (with β percentage difference in ECIC:
170 5.4 ± 1.8 %, $p < 0.01$; DCIC: 6.5 ± 2.5 %, $p < 0.05$, paired Student's t-test followed by Holm-
171 Bonferroni correction), but not CNIC (no significant difference).

172 During optogenetic stimulation, similar to the aversive vocalization experiment, the response
173 selectivity to the forward postejaculatory vocalizations was significantly enhanced throughout the
174 ascending auditory pathway (with the β percentage difference between forward and reversed
175 vocalization responses in IC: 19.2 ± 3.5 %, $p < 0.001$; MGB: 118.1 ± 43.0 %, $p < 0.01$; AC: 84.7
176 ± 23.2 %, $p < 0.001$, paired Student's t-test followed by Holm-Bonferroni correction). Specifically,

177 such enhancement primarily arose from increased responses to forward vocalizations (with β
178 percentage increase in forward vocalization response in IC: 15.2 ± 4.8 %, $p < 0.01$, MGB: 123.1
179 ± 36.6%, $p < 0.01$; AC: 74.7 ± 34.2 %, $p < 0.05$, paired Student's t-test followed by Holm-
180 Bonferroni correction). In IC, such increased responses were found in ECIC, DCIC as well as
181 CNIC (with β increase in ECIC: 16.0 ± 6.3 %, $p < 0.05$; DCIC: 9.8 ± 3.0 %, $p < 0.01$; CNIC: 17.3
182 ± 4.3 %, $p < 0.01$, paired Student's t-test followed by Holm-Bonferroni correction). Taken together,
183 these results demonstrate that the hippocampus plays a key role in modulating natural vocalization
184 processing. Such hippocampal modulatory effects are not biased towards the aversive content
185 embedded in the vocalizations. These fMRI findings again show that, for behaviorally relevant
186 sound, the hippocampal outputs triggered by the 5 Hz vHP stimulation enhance auditory
187 processing at large scale throughout the early ascending auditory pathway.

188 **Hippocampal outputs do not modulate neural responses to broadband acoustic noise**

189 To further investigate whether the modulatory effects of hippocampal outputs are only specific
190 to auditory processing of natural sounds, we replaced the vocalizations with a basic acoustic
191 stimulus, 1 – 40 kHz broadband noise (**Supplementary Figure 4**). As expected, the broadband
192 noise evoked BOLD responses along the ascending auditory pathway, including IC, MGB, and
193 AC. Importantly, the noise evoked BOLD responses in IC, MGB, and AC remained unchanged
194 during the vHP stimulation (**Figure 5**). This finding reveals that the hippocampal outputs do not
195 modulate behaviorally irrelevant or basic acoustic stimuli.

Pharmacological hippocampal inactivation alters auditory responses and their selectivity for vocalizations

In addition, we examined the effects of pharmacologically inactivating neurons in the dentate gyrus of vHP on natural sound processing using tetrodotoxin (TTX). Auditory fMRI was performed before (PRE) and after (POST) infusion of TTX at vHP (**Supplementary Figure 5**). As expected, before the TTX infusion, the BOLD responses evoked by aversive vocalizations showed response selectivity to the forward one (**Figure 6**) (with β percentage difference between forward and reversed vocalization responses in IC: 15.6 ± 1.9 %, $p < 0.01$; MGB: 77.6 ± 23.5 %, $p < 0.05$; AC: 132.2 ± 60.5 %, $p < 0.05$, paired Student's t-test followed by Holm-Bonferroni correction). Similarly, the response selectivity to forward aversive vocalizations in IC was mainly observed in ECIC and DCIC (with β percentage difference in ECIC: 11.2 ± 4.1 %, $p < 0.05$; DCIC: 31.4 ± 8.8 %, $p < 0.05$, paired Student's t-test followed by Holm-Bonferroni correction), but not in CNIC.

Notably, pharmacological vHP inactivation via TTX infusion abolished the response selectivity to forward aversive vocalizations throughout the ascending auditory pathway, including IC, MGB, and AC. In general, the BOLD responses to forward and reversed vocalizations were also reduced. Yet the BOLD responses to forward vocalizations were diminished by a much greater extent (with β percentage decrease in forward vocalization response in IC: -20.6 ± 3.9 %, $p < 0.01$; MGB: -54.4 ± 21.5 %, $p < 0.05$; AC: -44.9 ± 17.0 %, $p < 0.05$, paired Student's t-test followed by Holm-Bonferroni correction). In IC, such decreased responses were mainly found in ECIC and DCIC (with β percentage decrease in ECIC: -12.9 ± 3.9 %, $p < 0.05$; DCIC: -18.3 ± 3.6 %, $p < 0.01$, paired Student's t-test followed by Holm-Bonferroni correction), but not in CNIC. These findings present additional evidence that vHP modulates and shapes IC, MGB and AC response selectivity

219 to behaviorally relevant sounds at early sound processing centers within the ascending auditory
220 pathway.

221

222 ## Discussion

223 Here, we experimentally revealed the large-scale modulatory effects of ventral hippocampal
224 outputs on early sound processing within the ascending auditory pathway by monitoring auditory
225 responses during optogenetic vHP stimulation or pharmacological inactivation using large-view
226 fMRI. We discovered a robust hippocampal influence on BOLD responses to vocalizations, but
227 not artificial/basic acoustic stimuli, in the auditory midbrain, thalamus, and cortex. These fMRI
228 results directly support the large-scale and faciliatory influence of the hippocampus on natural
229 sound processing in early auditory centers within the ascending auditory pathway.

230 **Pathways subserving hippocampal top-down modulation of natural sound processing in**
231 **early auditory centers**

232 In the classical view, the auditory cortex processes complex auditory features and provides
233 corticofugal feedback to modulate the responses in IC and MGB (4, 19-22). In particular, the
234 existing hierarchical notion of cortical processing (48-50) postulates that the AC decodes the
235 spectrotemporal dynamic features of auditory inputs, which facilitate responses to complex natural
236 acoustic stimuli like vocalizations (5). However, studies suggest that complex sound processing
237 may also occur at early auditory centers (51, 52). Converging evidence indicates that extraction
238 and processing of spectral and temporal features begin at the midbrain level for discriminating
239 natural sounds (53, 54), such as vocalizations (46, 55, 56). Moreover, an electrophysiological study
240 showed that IC and MGB represent more comprehensive stimulus identities of natural stimuli

241 relative to the cortex (4), highlighting the importance of early auditory structures in processing
242 natural sounds. In addition, recent discoveries of non-canonical regions in processing complex
243 auditory stimuli, such as entorhinal cortex (Ent) and medial septum (MS) (19, 20), and inevitably
244 the hippocampus due to the dense reciprocal axonal projections (39, 57), challenge current dogma
245 on the hierarchical notion of cortical processing. Here, we directly demonstrated that the
246 hippocampus, a limbic region vital for learning and memory functions, modulates auditory
247 responses to natural sounds along the early ascending auditory pathway. We propose that the
248 hippocampus acts as a network hub that receives extensive projections from both subcortical and
249 cortical regions (38, 58). In this view, multiple complementary pathways likely subserve long-
250 range hippocampal modulation of central auditory processing of natural sound processing (**Figure**
251 **7**).

252 At the midbrain level, the IC integrates ascending auditory inputs from the lower auditory
253 structures and descending feedback signals from the auditory thalamus and cortex (3). Despite the
254 descending feedback from AC (24, 25), the IC also receives direct inputs from non-auditory
255 structures such as the amygdala (AMG) (29), a limbic region that interacts with the hippocampus
256 to regulate emotional memory (59, 60). The direct projection from AMG to IC may provide rapid
257 feedback for processing emotional auditory stimuli (61). Such AMG-IC projections provide a route
258 for vHP to modulate the responsiveness of IC neurons to specific types of stimuli based on the
259 behavioral relevance and emotional valence (29, 61). Meanwhile, a recent retrograde tracing study
260 revealed that IC receives descending projections from non-auditory regions, such as the entorhinal
261 (Ent), perirhinal (Prh), and cingulate (Cg) cortices (28). These regions are part of the hippocampal
262 formation and are linked with learning, memory, and sensory processes (31, 38, 62, 63). For
263 instance, the hippocampal-entorhinal circuit can acquire and discriminate frequency and temporal

features of auditory cues associated with reward-related behavior (20). Meanwhile, Prh inputs are required for fear conditioning to complex stimuli, such as vocalizations, but not for continuous tones (64, 65). Furthermore, the hippocampus also interacts with Cg to support memory encoding and retrieval of context-dependent information, thus facilitating the corresponding processing of behaviorally relevant stimuli (62, 63). Meanwhile, we found that our identified regions (AMG, Ent, Prh and Cg) were prominently activated upon 5 Hz optogenetic stimulation (**Figure 2**). Together, multiple afferents from non-auditory regions to IC suggest that inputs from higher-order structures, such as the vHP and its associated hippocampal formation, are vital for natural sound processing at the midbrain level.

At the thalamic level in the auditory hierarchy (66, 67), MGB can also receive hippocampal modulatory outputs via other sensory and prefrontal cortices, including somatosensory and cingulate cortices. For example, hind paw stimulation provides somatosensory inputs that can modulate auditory responses in the MGB (68), and electrical stimulation at the prefrontal cortex can influence spontaneous firing in the MGB (71). Meanwhile, MGB can also receive indirect inputs from the AMG via the thalamic reticular nucleus (TRN), which is critical for deviant sound detection (72). Exciting AMG-TRN projections amplified the sound-evoked responses in the auditory thalamus and, in turn, the cortex (73). Inactivating the basal AMG reduced certain conditioned responses to sound in MGB (74). Hence, the amplified sound-evoked response in MGB observed here can undergo modulation by hippocampal outputs via AMG and the prefrontal cortices such as cingulate.

At the cortical level, the auditory association area can receive hippocampal outputs directly from ventral CA1 neurons (41) and indirectly via the Ent, Prh, and parahippocampal cortices (75). Previous works have identified the functional roles of these hippocampal-cortical pathways

287 comprising auditory recognition (20, 76, 77) and auditory-related memory processes (33, 36).
288 Hippocampal modulatory outputs could potentially reach the auditory cortex through
289 hippocampal-cortical pathways (37), and subsequently also modulate sound responses in the
290 midbrain and thalamus via corticofugal projections (7, 23).

291 Recent evidence indicates that the reticular limbic auditory pathway may provide a fast route
292 to relay auditory inputs from the cochlear nucleus to high-order regions (19), suggesting that the
293 hippocampus receives and processes behaviorally relevant auditory inputs via Ent and MS. Further,
294 our histological findings showed strong anterograde ChR2 mCherry expression in the MS and
295 lateral septum (LS), as well as the diagonal band of Broca (DBB) (**Supplementary Figure 1B**),
296 suggesting a circuit loop that is dedicated for auditory processing outside of the central pathways.
297 These regions support learning (78) and memory functions (79), particularly related to auditory
298 processes. For instance, MS inactivation impairs acquiring auditory fear memory (22). MS and
299 DBB are the primary sources of cholinergic projections to HP and AMG (80), which can be critical
300 for contextual memory formation (81), sensory cue detection and discrimination (82, 83).
301 Disrupting MS and DBB cholinergic projections to vHP prevents auditory fear memory acquisition
302 and retention (84). Further, a prior study showed that systemic blockade of cholinergic signaling
303 via atropine, a muscarinic acetylcholine receptor antagonist, inhibited response selectivity to
304 vocalizations in the auditory midbrain (46). Here, robust activations in the septum complex (i.e.,
305 MS, LS, and DBB) initiated from vHP (**Figure 2**) may trigger rapid downstream signaling
306 cascades in the cholinergic system (82) and evoke postsynaptic responses at the terminal fields
307 (85), such as the AMG. Cholinergic signaling within AMG is crucial for encoding and processing
308 emotionally salient memories (86), which could facilitate selective amplification of auditory
309 responses evoked by behaviorally relevant stimuli. Overall, we detected robust activations in

cortical (i.e., AC, Ent, Prh, Cg) and subcortical regions (i.e., AMG, MS, LS, DBB) during 5 Hz optogenetic stimulation at vHP (**Figure 2**). The hippocampal modulatory outputs evoked from vHP could propagate and functionally interact with these activated regions, thereby modulating auditory responses at early auditory centers within the ascending auditory pathway, particularly at the midbrain and thalamic levels.

Hippocampal outputs enhance natural sound responses at early auditory centers

In this study, we revealed that optogenetic activation of vHP, a region often associated with motivation or emotional behaviors (42, 43), enhanced auditory responses in early ascending auditory processing centers (i.e., IC, MGB) and the AC to forward, but not temporally reversed, vocalizations. Pharmacological inactivation of vHP diminished the auditory responses to forward vocalizations. Further, such hippocampal modulatory effects were absent when processing broadband noise, confirming that hippocampal activity is an integral component of natural sound processing within the ascending auditory pathway. Our findings demonstrate that the hippocampus is key for processing vocalizations and shaping the corresponding response selectivity.

The exact mechanisms underlying our experimentally observed selective modulation of natural sound processing by optogenetically triggered hippocampal outputs requires further investigation. We posit that specific spectrotemporal information embedded in the sound drive this specificity. The hippocampus is positioned to process temporal information of sensory inputs (33, 93), as hippocampal lesions can impair memory for the temporal order of events in both animals (94, 95) and humans (96, 97). When learning to associate specific time intervals with a given stimulus, the hippocampus is essential for discriminating minute temporal differences in rodents (98). These findings indicate that the hippocampus plays a critical role in encoding and recognizing temporal

information to subsequently discriminate and interpret the temporal organization of incoming sensory inputs.

Here, we observed that hippocampal modulation primarily facilitates auditory responses in IC, MGB, and AC to both types of vocalizations (i.e., aversive/fear and postejaculatory/positive), but not their temporally reversed counterparts (**Figures 3** and **4**). We postulate that temporally reversing vocalizations alter specific properties. Reversed vocalizations no longer carry the critical information embedded in forward vocalizations, which diminishes the behavioral relevance of the sound. The hippocampus, by interpreting and discriminating the embedded spectrotemporal features of the incoming sounds, can discriminate and recognize natural and/or behaviorally relevant stimuli by contextual memory recall according to past experience (99, 100) and then can exert selective influence to downstream targets. Moreover, blocking hippocampal outputs through pharmacological manipulation altered responses to forward vocalizations, and consequently disrupted the response selectivity to vocalizations (**Figure 6**). Together, our results showed that hippocampal outputs are critical to facilitate auditory responses to natural sounds.

Hippocampal modulatory outputs, such as the increased coherence of neuronal firing with theta/gamma oscillations (101) and/or modifying synaptic strengths (102), can promote communication between the hippocampus and its downstream targets, and then facilitate natural sound processing via multiple pathways. At a systems level, theta oscillations can correspond to contextual memory recall (i.e., retrieval of contextual information pertaining to a specific event in the past where its temporal context or sequence is important) (103-105). During memory retrieval, theta oscillations coupled with gamma oscillations were enhanced when processing previously learned, behaviorally relevant stimuli (106). We speculate that optogenetically initiated hippocampal outputs generate theta-like oscillations in the hippocampal-cortical network (44, 45)

to enhance retrieval processes between the hippocampus and Ent during auditory processing. Previous studies also demonstrated the importance of hippocampal and cortical theta oscillations (101, 107) in coordinating groups of neurons to integrate sensory information (108). Theta oscillations are essential to coordinate brain-wide activity (109), such that neuronal spiking in somatosensory (110), prefrontal (111) and entorhinal cortices (112) are phase-locked to hippocampal theta oscillations. These studies indicate that the hippocampus can influence distal sensory responses via theta oscillations.

In this study, we uncovered long-range hippocampal modulation of natural sound processing within the ascending auditory pathway during 5 Hz optogenetic stimulation at vHP. This stimulation frequency coincides with the reported range of hippocampal theta oscillations (101, 107), evoked the most robust brain-wide activations, including in primary AC. Such theta-like activities could trigger the propagation of hippocampal activity to distal regions, facilitating the interaction with neural activity in the ascending auditory pathway (i.e., AC, MGB and IC) and other targets to produce modulatory effects. However, we do not preclude the potential modulatory effects of other stimulation frequencies in the range of theta oscillations like 10 Hz (101, 107). Even though BOLD activations evoked by 10 Hz optogenetic stimulation were not as widespread as 5 Hz, we still observed robust activations in subcortical regions (e.g., AMG, MS, LS, DBB) albeit with weaker activations in cortical regions (e.g., AC, Prh, Cg) (**Supplementary Figure 2**). Overall, our findings suggest that hippocampal top-down modulatory outputs, which may be triggered by behaviourally relevant auditory inputs, were augmented by optogenetic stimulation of vHP to enhance responses to natural sounds.

In summary, the present fMRI study established a top-down and large-scale modulatory role for the hippocampus throughout the ascending auditory pathway, including the auditory midbrain,

thalamus and cortex, to faciliate natural sound processing. Our findings expand our present understanding of central auditory system beyond the traditional cortex centric views. Future studies should elucidate the precise hippocampal modulatory processes of natural sound that arise from the brain-wide auditory information processing networks.

Methods

Subjects

Adult male Sprague-Dawley rats were used in all experiments. Animals were individually housed under a 12-h light/dark cycle with access to food and water ad libitum. All animal experiments were approved by the Committee on the Use of Live Animals in Teaching and Research of the University of Hong Kong. Group I underwent optogenetic fMRI experiments (n = 10), group II underwent combined optogenetics and auditory fMRI experiments (n = 11, aversive vocalizations experiments; n = 10, postejaculatory vocalizations experiments; n = 8, broadband noise experiments), and group III underwent combined pharmacological and auditory fMRI experiments (n = 7, aversive vocalizations experiments). Full details of animal surgical procedures, optogenetic stimulation paradigms, combined optogenetics, and auditory fMRI acquisition and analysis procedures, and histology are provided in SI Methods.

Data and Code Availability

The data files that support the findings of this study and computer codes used are available on Dryad Digital repository (https://doi.org/10.5061/dryad.08kprr52x).

Acknowledgments

This work was supported by Hong Kong Research Grant Council (C7048-16G and HKU17112120 to E.X. Wu, and HKU17103819 and HKU17104020 to A.T.L. Leong), Lam Woo Foundation, Guangdong Key Technologies for Treatment of Brain Disorders (2018B030332001) and

Guangdong Key Technologies for Alzheimer's Disease Diagnostic and Treatment (2018B030336001) to E.X. Wu. We would like to thank Profs. J. He and G. Buzsáki for the insightful scientific discussions. We also thank Drs. R. Chan, C. Dong, A. To, and M. Bialy for their technical assistance. We also thank Dr. K. Deisseroth who provided us with the ChR2 viral construct.

Competing Financial Interests

The authors declare no competing financial interests.

Figures

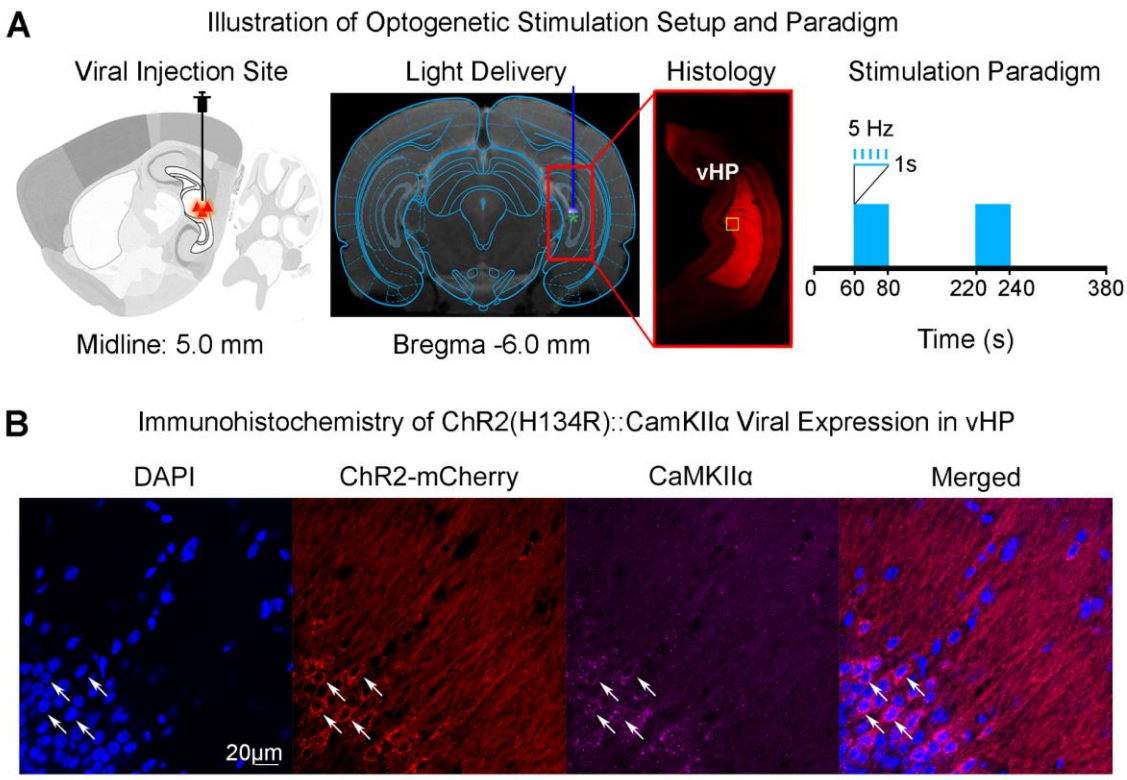

Figure 1. Experimental setup for optogenetic stimulation and histological characterization of ChR2::CaMKII viral expression in ventral hippocampus (vHP) excitatory neurons. ***(A)*** Schematic *(Left)* and T2-weighted anatomical image *(Middle)* shows the viral injection and fiber implantation sites, respectively. Histology image shows viral expression in vHP (Red box). The yellow box indicates the location of magnified confocal images shown in *B*. Optogenetic fMRI stimulation paradigm *(Right)*. 5 Hz was presented at 30 % duty cycle in a block-design paradigm (20 seconds ON; 140 seconds OFF). ***(B)*** Merged representative confocal images co-stained for the nuclear marker DAPI, ChR2-mCherry, and excitatory marker CaMKIIα confirmed colocalization of ChR2-mCherry and CaMKIIα^{+} neurons of vHP (white arrows).

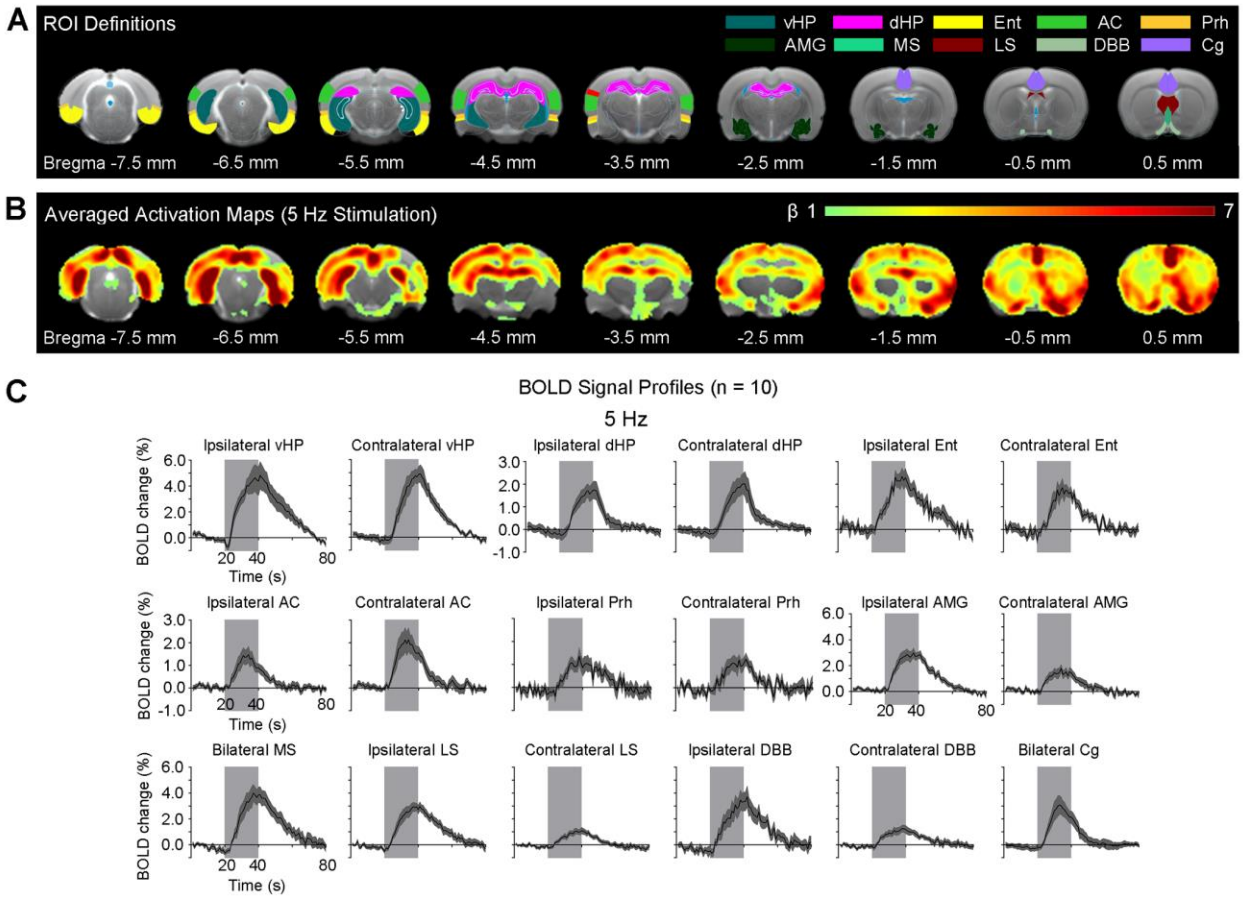

Figure 2. Brain-wide activations detected in the hippocampal formation, and cortical and subcortical regions during 5 Hz optogenetic stimulation of excitatory neurons in vHP. ***(A)*** Regions of interest (ROIs) defined by the rat brain atlas used to extract the BOLD signal profiles. ***(B)*** Averaged activation (β) maps of optogenetic stimulation in vHP. Robust positive BOLD responses detected in bilateral vHP, dHP, Ent, AC, Prh, AMG, MS, LS, DBB, and Cg during 5 Hz optogenetic stimulation ($n = 10$; $t > 3.1$; corresponding to $p < 0.001$). ***(C)*** BOLD signal profiles extracted from the ROIs. Error bars indicate ± SEM. The area shaded in grey indicates the 20 s 5 Hz optogenetic stimulation window. Abbreviations: Ventral Hippocampus (vHP); Dorsal Hippocampus (dHP); Entorhinal Cortex (Ent); Auditory Cortex (AC); Perirhinal Cortex (Prh); Amygdala (AMG); Medial Septum (MS); Lateral Septum (LS); Diagonal Band of Broca (DBB); Cingulate Cortex (Cg).

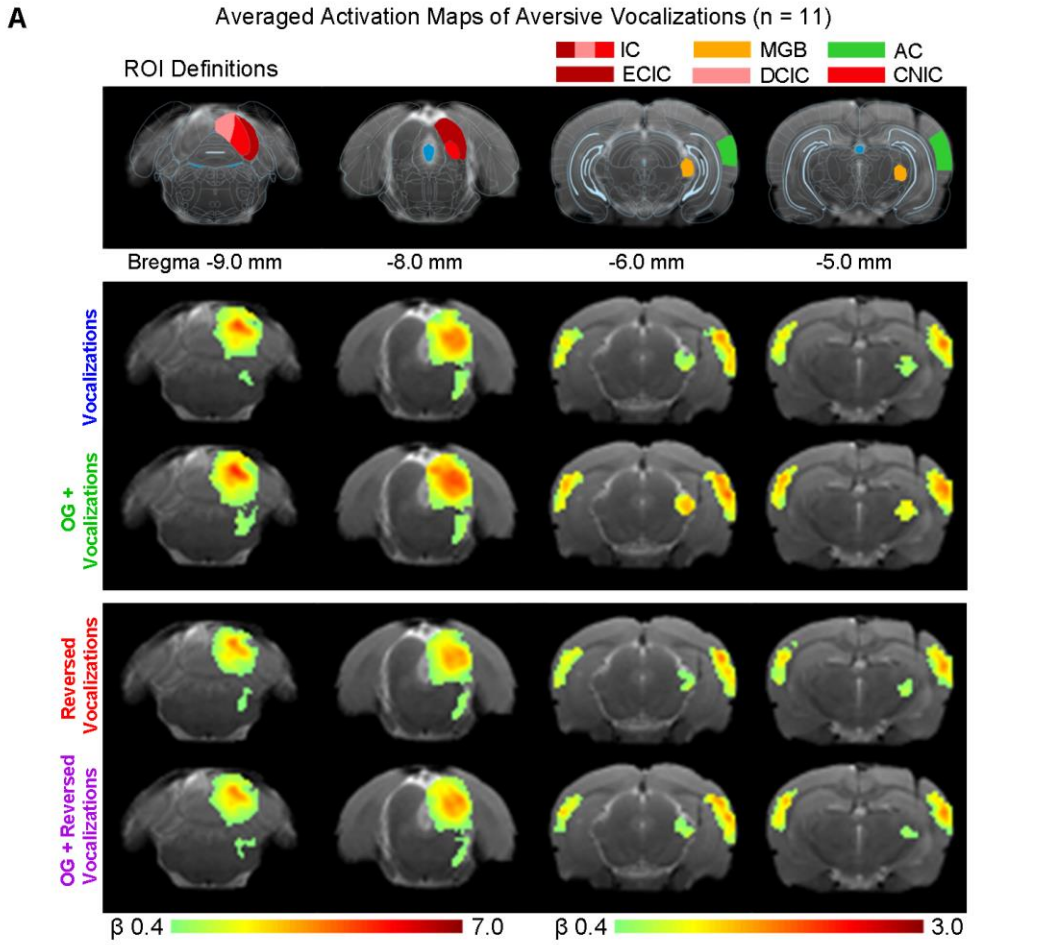

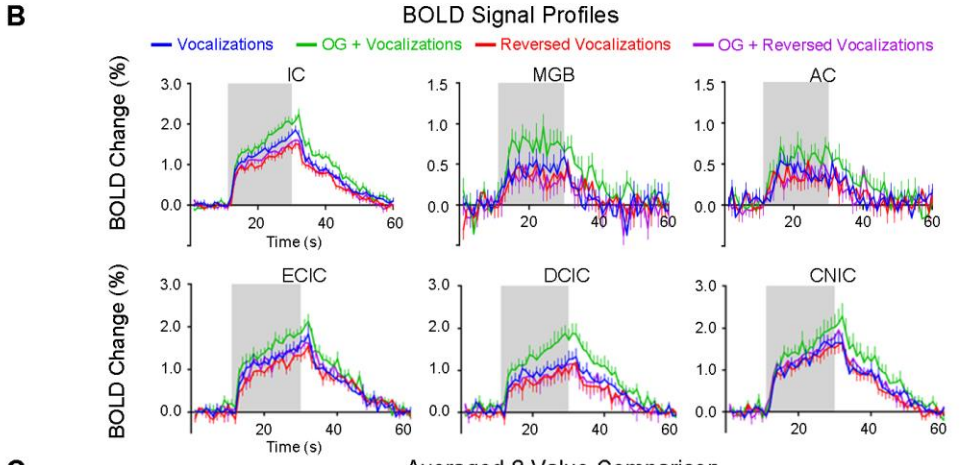

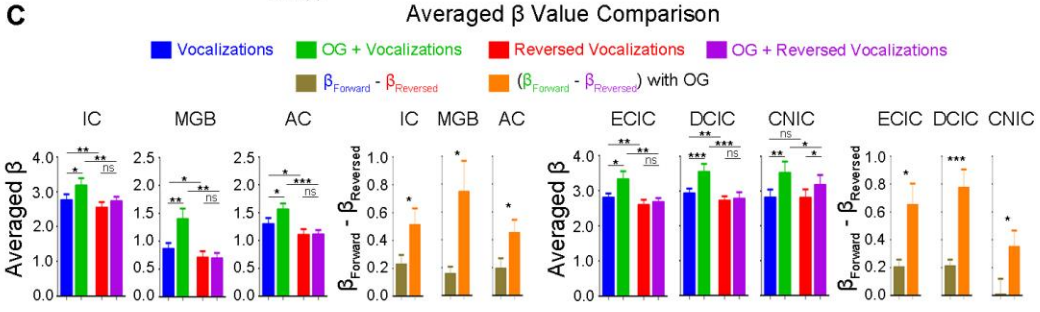

433

Figure 3. vHP optogenetic stimulation enhances neural responses and their selectivity to aversive vocalizations in the auditory midbrain (inferior colliculus or IC), thalamus (medial geniculate body or MGB), and cortex (auditory cortex or AC). ***(A)*** Illustration of the atlas-based region of interest (ROI) definitions *(Top)***.** Averaged BOLD activation (β) maps with and without 5-Hz optogenetic stimulation generated by fitting a canonical hemodynamic response function (HRF) to individual voxels in the fMRI image ($n = 11$; $t > 2.6$; corresponding to $p < 0.01$) *(Bottom)*. ***(B)*** BOLD signal profiles extracted from the corresponding ROIs (IC, MGB, AC, ECIC, DCIC, and CNIC). Error bars indicate ± SEM. The area shaded in grey indicates the 20 s acoustic stimulation. ***(C)*** BOLD signal (averaged β) comparison showing the modulatory effects of optogenetic stimulation on responses to forward aversive vocalizations in IC, MGB, AC, ECIC, DCIC, and CNIC, but not temporally reversed counterparts (that are artificial and evoke no behavioral response). Statistical comparisons were performed using paired two-sample t-test followed by Holm-Bonferroni correction with * for $p < 0.05$, ** for $p < 0.01$, *** for $p < 0.001$, and n.s. for not significant.

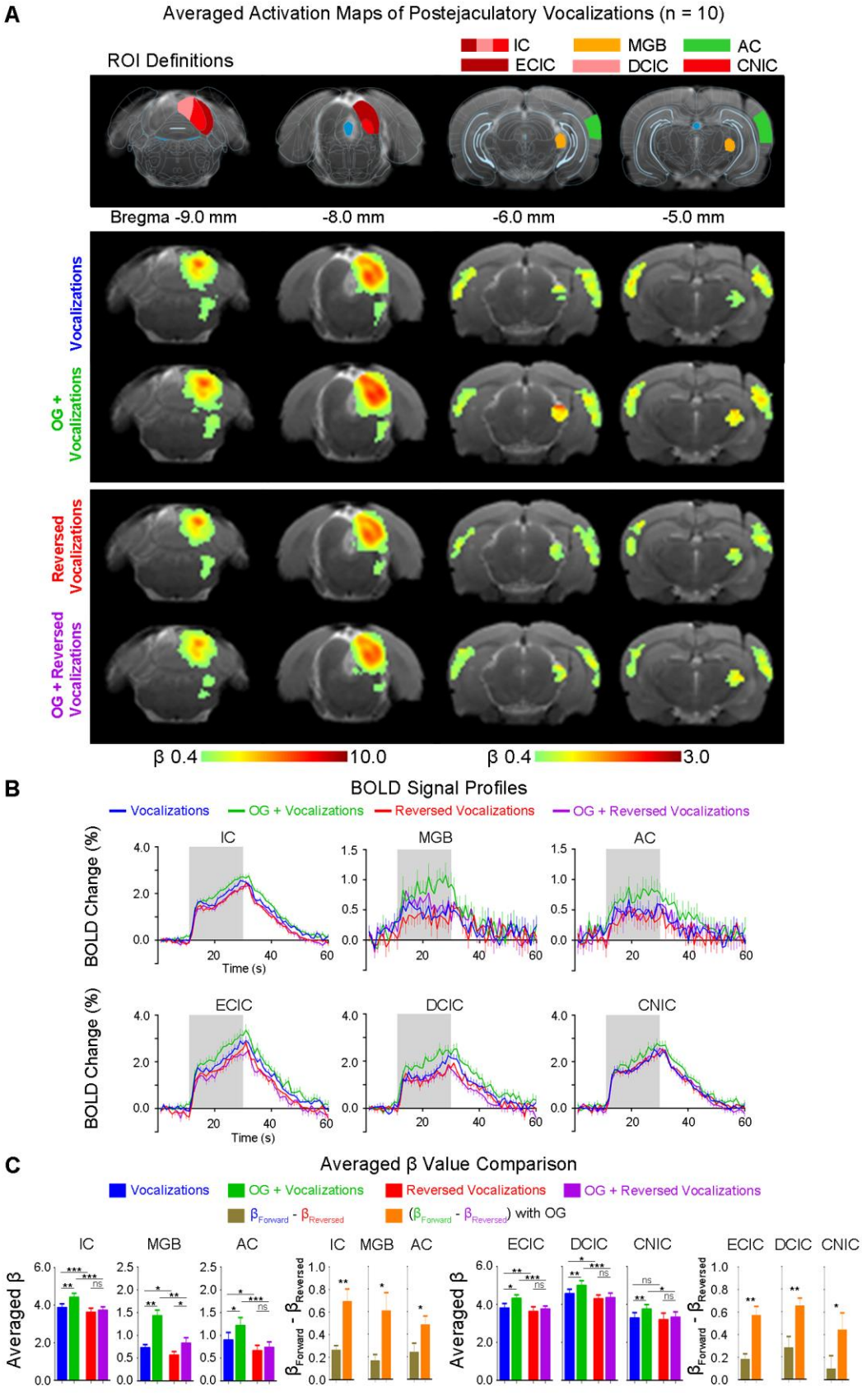

447

Figure 4. vHP optogenetic stimulation enhances neural responses and their selectivity to postejaculatory vocalizations in the auditory midbrain (IC), thalamus (MGB), and cortex (AC). ***(A)*** Illustration of the atlas-based region of interest (ROI) definitions *(Top)*. Averaged BOLD activation (β) maps with and without 5-Hz optogenetic stimulation *(Bottom)* generated by fitting a canonical HRF to individual voxels in the fMRI image ($n = 10$; $t > 2.6$; corresponding to $p < 0.01$). ***(B)*** BOLD signal profiles extracted from the corresponding ROIs (IC, MGB, AC, ECIC, DCIC, and CNIC). Error bars indicate ± SEM. The area shaded in grey indicates 20 s acoustic stimulation. ***(C)*** BOLD signal (averaged β) comparison showing the modulatory effects of optogenetic stimulation on responses to forward postejaculatory vocalizations in IC, MGB, AC, ECIC, DCIC, and CNIC, but not the temporally reversed counterparts. Statistical comparisons were performed using paired two-sample t-test followed by Holm-Bonferroni correction with * for $p < 0.05$, ** for $p < 0.01$, *** for $p < 0.001$, and n.s. for not significant.

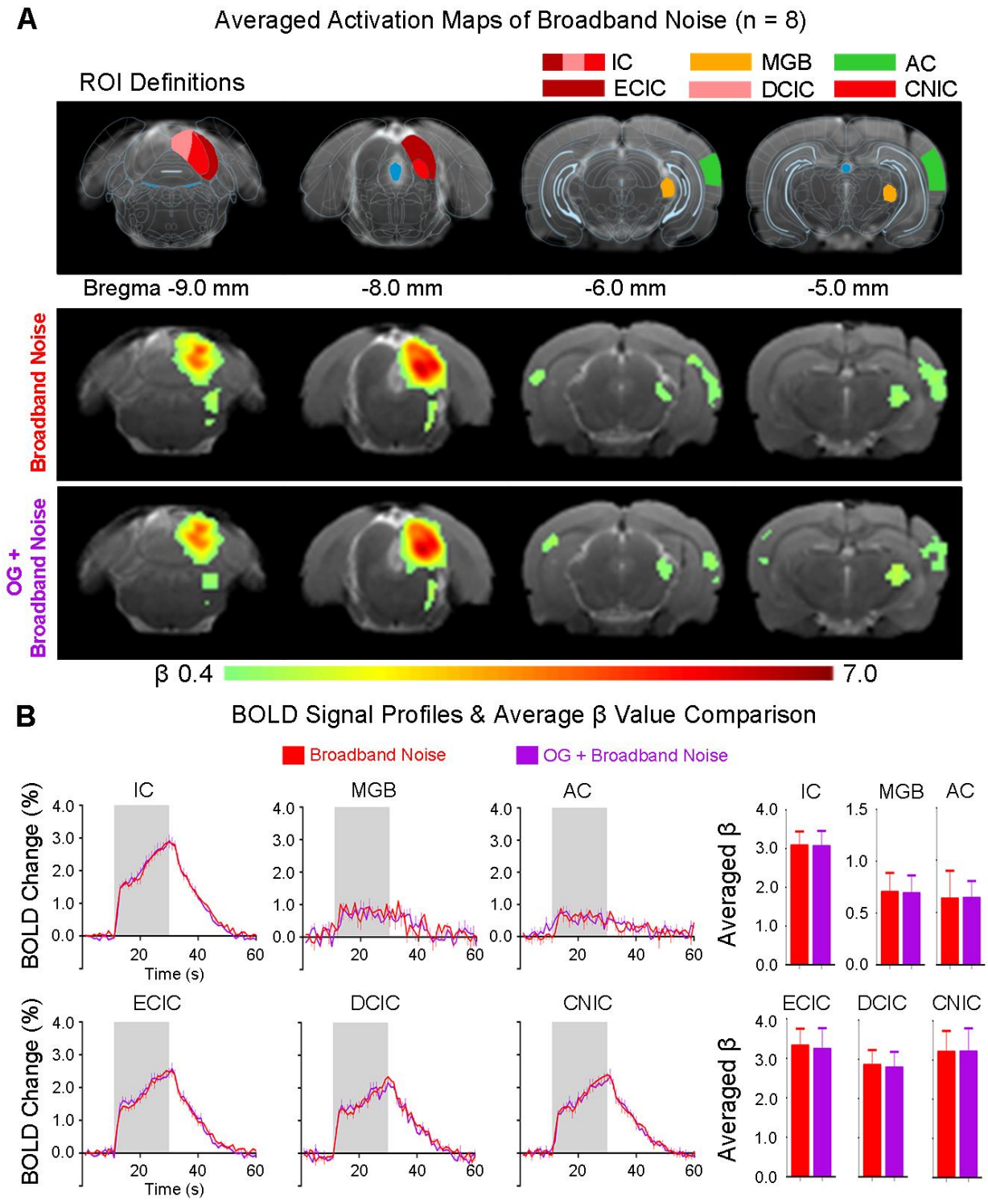

459

460 **Figure 5. vHP optogenetic stimulation shows no modulatory effects on the responses to broadband**

461 **acoustic noise in the auditory midbrain (IC), thalamus (MGB), and cortex (AC).** ***(A)*** Illustration of the

462 atlas-based region of interest (ROI) definitions *(Top)*. Averaged BOLD activation (β) maps with, without
463 5-Hz optogenetic stimulation *(Bottom)* generated by fitting a canonical HRF to individual voxels in the
464 fMRI image ($n = 8$; $t > 2.6$; corresponding to $p < 0.01$). ***(B)*** BOLD signal profiles *(Left)* extracted from the
465 corresponding ROIs (IC, MGB, AC, ECIC, DCIC, and CNIC). Error bars indicate ± SEM. The area shaded
466 in grey indicates the 20 s acoustic stimulation. BOLD signal (averaged β) comparison *(Right)* showing no
467 effects of optogenetic stimulation on broadband noise responses in IC, MGB, and AC. Statistical
468 comparisons were performed using paired two-sample t-test followed by Holm-Bonferroni correction.

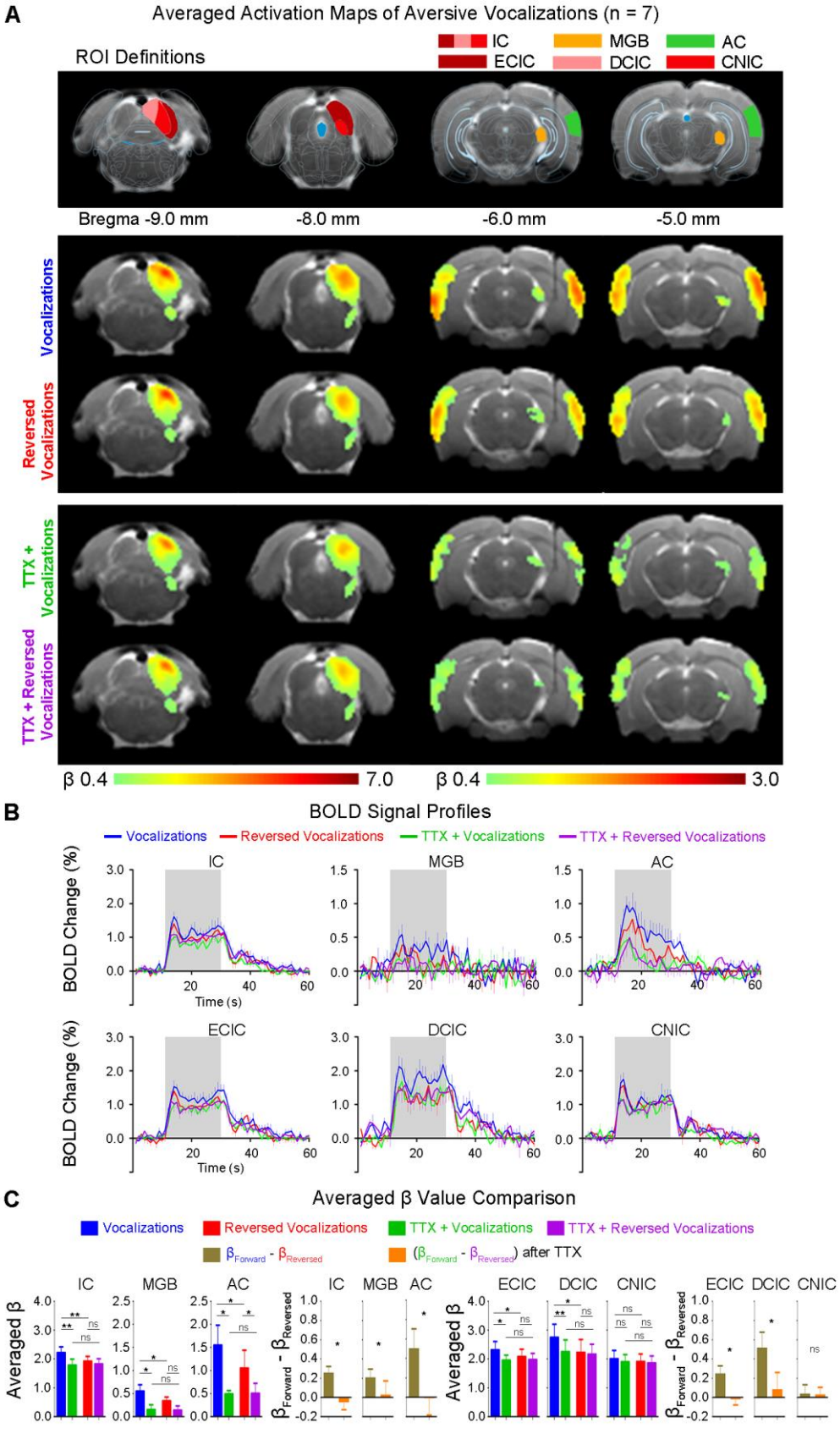

469

Figure 6. Pharmacologically inactivating vHP alters neural responses and decreases their selectivity to aversive vocalizations in the auditory midbrain (IC), thalamus (MGB), and cortex (AC). ***(A)*** Illustration of the atlas-based region of interest (ROI) definition *(Top)*. Averaged BOLD activation (β) maps before and after TTX infusion *(Bottom)* generated by fitting a canonical hemodynamic response function (HRF) to individual voxels in the fMRI image ($n = 7$; $t > 2.6$; corresponding to $p < 0.01$). ***(B)*** BOLD signal profiles extracted from the corresponding ROIs (IC, MGB, AC, ECIC, DCIC, and CNIC). Error bars indicate ± SEM. The area shaded in grey indicates 20 s acoustic stimulation. ***(C)*** BOLD signal (averaged β) comparison showing the effects of TTX inactivation of vHP neurons predominantly on responses to forward aversive vocalizations in IC, MGB, AC, ECIC, and DCIC. Statistical comparisons were performed using paired two-sample t-test followed by Holm-Bonferroni correction with * for $p < 0.05$, ** for $p < 0.01$, *** for $p < 0.001$, and n.s. for not significant.

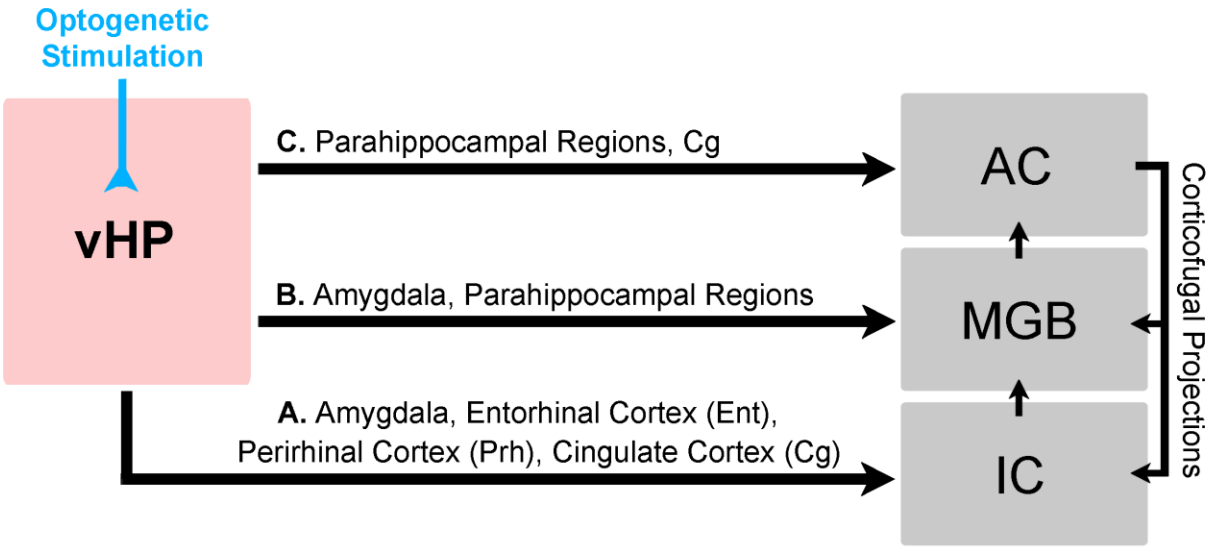

Figure 7. Schematic pathways of long-range hippocampal modulation of natural sound processing within the ascending auditory pathway through optogenetically-evoked vHP activity. ***Route A:*** vHP could modulate responses in IC via indirect projections from amygdala, entorhinal cortex (Ent), perirhinal cortex (Prh) and cingulate cortex (Cg), which can then enhance the responses in MGB and AC along the ascending auditory pathway. ***Route B:*** vHP can modulate MGB responses indirectly via amygdala and parahippocampal regions, which could subsequently modulate responses in AC via ascending auditory pathway. ***Route C:*** vHP could modulate AC responses directly via hippocampal-cortical projections or indirectly via parahippocampal regions such as Ent, Prh, and Cg via cortico-cortical projections. AC could then modulate the responses in MGB and IC via corticofugal projections.

SI Appendix

Hippocampus Modulates Natural Sound Processing at Early Auditory Centers

Eddie C. Wong[1,2], Xunda Wang[1,2], Ed X. Wu[1,2,3*], Alex T. L. Leong[1,2*]

[1]Laboratory of Biomedical Imaging and Signal Processing, The University of Hong Kong, Pokfulam, Hong Kong SAR, China

[2]Department of Electrical and Electronic Engineering, The University of Hong Kong, Pokfulam, Hong Kong SAR, China

[3]School of Biomedical Sciences, LKS Faculty of Medicine, The University of Hong Kong, Pokfulam, Hong Kong SAR, China

[*]Correspondence should be addressed to Ed X. Wu, Ph.D. and Alex T. L. Leong, Ph.D.:

Laboratory of Biomedical Imaging and Signal Processing, Department of Electrical and Electronic Engineering, School of Biomedical Sciences and Department of Medicine, The University of Hong Kong, Pokfulam, Hong Kong, Hong Kong SAR, China.

Fax: +852-2859-8738.

Tel: +852-2859-7096.

Email: ewu@eee.hku.hk & tlleong@eee.hku.hk

SI Methods

Virus Packaging

Channelrhodopsin2-mCherry fusion protein under the control of the Ca^{2+} /calmodulin-dependent protein kinase IIα (CaMKIIα) promoter was used. The AAV5-CaMKIIα-ChR2(H134R)-mCherry plasmid (maps available online from www.stanford.edu/group/dlab/optogenetics) was packaged by the viral vector core of the University of North Carolina at Chapel Hill, Chapel Hill, NC (tire of 4 x 10^{12} particles/mL).

Stereotactic Surgery for Viral Injection

Stereotactic surgery was performed when rats were 6 weeks old with bodyweight around 250 g. Rats were anesthetized with an intraperitoneal bolus injection of ketamine (90 mg/kg) and xylazine (40 mg/kg) mixture. The scalp was shaved, and the rats were secured in a stereotactic frame. Buprenorphine (0.05 mg/kg) was administered subcutaneously to minimize pain, and heating pads were used to prevent hypothermia. Following a midline incision, a craniotomy was made on the right hemisphere in the vHP, and injection was performed at two depths (-6.00 mm posterior to Bregma, +5.00 mm ML, -4.75 and -4.50 mm from brain surface). For optogenetic animals, 1.5 µL of viral constructs were delivered through a 5 µL syringe and 33-gauge beveled needle injected at 150 nL/min at each depth. Following viral injection, the needle was held in the place for 10 minutes before slow retraction. Then, the scalp incision was sutured. After the surgery, buprenorphine (0.05 mg/kg) was administered subcutaneously twice daily for 72 hours to minimize post-surgery infection and inflammation. Animals rested for six weeks before fMRI experiments were performed.

Optical Fiber Implantation

Stereotactic surgery was performed to implant custom made plastic optical fiber cannula (POF, core diameter 450 μm; Mitsubishi Super ESKA^{TM} CK-20) at the viral injection site 1 – 2 hours before fMRI experiments. Rats were anesthetized with isoflurane (induction 3 % and maintenance 2 %) and secured on a stereotactic frame. Following a midline incision, a craniotomy was made at the same coordinates as the viral injection site. A heating pad was used to prevent hypothermia. Before implantation, the fiber tip was beveled to facilitate insertion and minimize injury to brain tissue. Then, it was inserted with the fiber tip at a depth of 4.7 mm. The optical fiber was fixed on the skull with UV glue and dental cement, and the scalp incision was sutured. The fiber outside the brain was made opaque using heat-shrinkable sleeves to avoid undesired visual stimulation. After the surgery, buprenorphine (0.05 mg/kg) was administered subcutaneously to minimize discomfort.

Cannula Implantation for Tetrodotoxin (TTX) Infusion

Before animals were placed in the magnet, surgery was performed to implant an MRI-compatible cannula, 250-μm internal diameter in vHP. Before surgery, animals were anesthetized with isoflurane (induction 3% and maintenance 2%) secured on a stereotactic frame. Buprenorphine (0.05 mg/kg) was administered subcutaneously to minimize discomfort before MRI experiments. The concentration of TTX used was 5-10 ng/μL, similar to the values used in previous in vivo studies (113, 114).

Animal Preparation for MRI Experiments

All MRI experiments were carried out on a 7T MRI scanner (PharmaScan 70/16, Bruker Biospin) using a transmit-only birdcage coil in combination with an actively decoupled receive-only surface

coil. After surgery, one to two drops of 2% lidocaine was applied to the chords to provide local anesthesia before endotracheal intubation. The animals were mechanically ventilated at a rate of 60 breaths per minute with 1–1.5% isoflurane in room-temperature air using a ventilator (TOPO, Kent Scientific). During all fMRI experiments, animals were placed on a plastic cradle with the head fixed with a tooth bar and plastic screws in the ear canals. Rectal temperature was maintained at ~37.0 °C using a water circulation system. Continuous physiological monitoring was performed using an MRI-compatible system (SA Instruments). Vital signs were within normal physiological ranges (rectal temperature: 36.5 – 37.5 °C, heart rate: 350 – 420 beat/min, respiration rate: 60 breath/min, oxygen saturation: > 95%) throughout the experiments.

MRI-Synchronized Optogenetic and Auditory Stimulation

An Arduino programming board synchronized the scanner trigger and the lasers for optogenetic and visual stimulation. Computers and light delivery systems were kept outside the magnet, and long optical patch cables (5–10 m) delivered light into the bore of the scanner. For optogenetic stimulation, blue light was delivered using a 473-nm DPSS laser. Light intensity was measured (PM100D, Thorlabs, USA) before each experiment as 8 mW at the fiber tip (450 μm, NA = 0.5), corresponding to a light intensity of 40 mW/mm^2. For auditory stimulation, acoustic stimuli were controlled by a computer and produced by a high frequency multi-field magnetic speaker (MF1, TDT) driven by an amplifier (SA1, TDT). Monaural stimulation was delivered through a custom-made 165 cm long rigid tube and a 6.5 cm soft tube into the animals' left ear canal. The right ear was occluded with cotton and Vaseline, to reduce the scanner noise reaching the ears. The sound pressure level (SPL) was measured by a recorder (FR2, Fostex, Japan) placed at ~ 2 mm from the tip of the soft tube. The variance of the light power was maintained less than 2.5 mW/mm^2 and the SPL less than 2 dB. This setup has been used in our previous studies (46, 115).

To determine the frequency-dependent spatiotemporal characteristics of evoked vHP responses (optogenetic fMRI experiments), five frequencies were used (1 Hz, 5 Hz, 10 Hz, 20 Hz, and 40 Hz) with a light intensity of 40 mW/mm^2. 30 % duty cycle was used for all stimulation frequencies, except 1 Hz, which was at 10 % duty cycle. The duty cycle for 1 Hz optogenetic stimulation was reduced to avoid a very long stimulation pulse width which may not be physiological. vHP excitatory neurons were stimulated with a block design paradigm that consisted of 60 seconds light-off followed by 20 seconds light-on and 140 seconds light-off periods. Three to four trials were recorded for each frequency in an interleaved manner in each animal.

In combined optogenetic and auditory fMRI experiments, the effects of optogenetic stimulation in the vHP on brain baseline BOLD signals were examined by presenting 5 Hz stimulation (60 seconds light-off followed by 20 seconds light-on and 140 seconds light-off periods), without presenting acoustic stimulation. This paradigm was repeated twice in each animal. Subsequently, the effects of optogenetic stimulation on auditory midbrain, thalamus, and cortex processing of sound stimulation were investigated.

In the vocalization experiment, two types of vocalizations (I. 'Aversive' Vocalizations: bandwidth: 22-25 kHz, peak frequency: 22 kHz; sound pressure level (SPL): 83 dB, obtained online from http://www.avisoft.com/rats.htm (46); II. 'Postejaculatory' Vocalizations: bandwidth: 22 kHz, peak frequency: 22 kHz; SPL: 83 dB) from (91) and their temporal reversions were presented. Standard block-design paradigm was used for the auditory stimulation (40 s sound-off followed by 4 blocks of 20 s sound-on and 40 s sound-off, fMRI no. of time points = 280). During every 20 s sound-on period, the aversive vocalization (length 1.2 s, plus silence 0.8 s afterward) was repeated ten times at 60 % duty cycle, whereas the postejaculatory vocalization (length 3.6 s, plus silence 0.4 s afterward) were repeated five times at 90 % duty cycle. For each animal, this

603 paradigm was repeated six times for each type of vocalization sounds. For three of them, the
604 forward vocalization was presented first; and for the other three, the reversed one was presented
605 first. Note that the forward and temporally reversed vocalizations contained identical acoustic
606 features except reversed temporal information (**Supplementary Figure 3**). Note that temporally
607 reversed vocalizations were employed here as the control for forward (i.e., true and behaviorally
608 relevant) vocalizations. Such temporally reversed vocalizations exhibited the identical sound
609 pressure level (SPL that is important to BOLD response level), but triggered minimal behavioral
610 responses (46).

611 In the control experiment, broadband noise (bandwidth: 1 – 40 kHz; SPL: 83 dB) was presented
612 to the left ear canal of the animals in a standard block-design paradigm (40 seconds sound-off
613 followed by four blocks of 20 seconds sound-on and 40 seconds sound-off, fMRI no. of time points
614 = 280) (**Supplementary Figure 4**). During each 20 seconds sound-on period, the broadband noise
615 was presented with amplitude modulation at 4 Hz and 80 % duty cycle. The optogenetic
616 stimulation (light wavelength: 473 nm, intensity: 40 mW/mm^2, pulse rate: 5 Hz, duty cycle: 30%)
617 was continuously presented to the right vHP throughout the auditory fMRI sessions and alternated
618 between sessions.

619 In combined TTX and auditory fMRI experiment, a total of sixteen auditory fMRI sessions
620 were performed in each animal. After eight sessions, 5μL TTX (concentration: 5-10 ng/μL) (113,
621 114) was infused into vHP. The next immediate session was then acquired one minute after the
622 TTX infusion. During auditory fMRI sessions, auditory stimuli were presented to the left ear canal
623 of the animals. Aversive vocalization and its temporal reversion were presented in standard block
624 design paradigm (40 s sound-off followed by 4 blocks of 20 s sound-on and 40 s sound-off, fMRI
625 no. of time points = 280). Auditory fMRI sessions were interleaved (i.e., either starting with

626 forward aversive vocalization or temporally reversed aversive vocalization; **Supplementary**
627 **Figure 5**).

628 **MRI Acquisitions**

629 Scout images were first acquired to determine the coronal and sagittal planes of the brain.
630 Twelve coronal slices with 1.0 mm thickness were positioned to cover the ascending auditory
631 pathway with the 2nd, and 3rd slice covered the whole IC. T2-weighted images were acquired as
632 anatomical reference using a Rapid Acquisition with Refocused Echoes (RARE) sequence (FOV
633 = 32 x 32 mm^2, data matrix = 256 x 256, RARE factor = 8, echo time (TE) = 36, repetition time
634 (TR) = 4200 ms). All fMRI measurements were obtained using a multi-slice single-shot Gradient-
635 Echo Echo-Planar-Imaging (GE-EPI) sequence (FOV = 32 x 32 mm^2, data matrix = 64 x 64, flip
636 angle = 56°, TE/TR = 20/1000 ms, temporal resolution = 1000ms). Note that the fiber outside was
637 made opaque using heat-shrinkable sleeves to avoid unwanted visual stimulation.

638 **fMRI Data Analysis**

639 For each animal, the fMRI images from each animal were realigned to the mean image of the
640 first fMRI session (SPM12, Wellcome Department of Imaging Neuroscience, University College
641 London, UK). Images from each animal were co-registered to a custom-made brain template using
642 affine transformation and Gaussian smoothing, with the criteria of maximizing normalized mutual
643 information (SPM12). For optogenetic fMRI and auditory fMRI, data from repeated sessions were
644 averaged, in-plane smoothed (FWHM = 1 pixel), and high-pass filtered (128 s), and then standard
645 general linear model (GLM) was applied, to calculate the BOLD response coefficient (β) maps for
646 each stimulus (SPM12). fMRI sessions suffering from motion artifacts (>0.125 mm voxel shifts
647 detected by realignment) and sudden physiological changes (i.e., abrupt changes in respiration

pattern, heart rate and oxygen saturation level) were discarded. Typically, in each animal, three fMRI sessions were averaged for vHP optogenetic stimulation only, whereas four sessions were averaged for combined auditory and vHP optogenetic stimulation. Finally, activated voxels were identified with Student's t-test on the β values ($p < 0.01$).

Three regions-of-interest (ROIs) covering different IC subdivisions were defined using the Paxinos & Watson rat brain atlas. The ROI that covered the inferior colliculus (IC), medial geniculate nucleus (MGB), or auditory cortex (AC) was defined by identifying clusters of activated voxels ($p < 0.05$) that were restricted within the anatomical location of each region. Anatomical locations of IC, MGB, and AC, were determined using the atlas. In individual animals, the BOLD signal profiles for each ROI were first extracted and averaged across voxels, before they were separated into six blocks (each covering a period from 10 s before to 30 s after a sound-on period) and two blocks (each covering a period from 10 s before to 50 s after an optogenetic-ON period), respectively. They were then averaged again and normalized by the mean signal intensity of the first 10 s to calculate the percentage of BOLD signal change. Final averaging was then performed across animals to generate BOLD signal profiles.

In individual animals, β values were also extracted from each ROI and averaged across voxels. The final β value used for comparison between the BOLD responses to the sound stimulus with and without optogenetic stimulation of the vHP was computed by averaging. Further, the β value difference between forward and reversed vocalizations ($\beta_{Forward} - \beta_{Reversed}$), as a metric of response selectivity, was compared between with and without optogenetic stimulation. Note that the size of ROI for each IC subdivision was different, and this could influence the absolute SNR of the averaged BOLD responses.

Histology, Immunohistochemistry, and Confocal imaging

671

672 Upon completion of in vivo studies, animals were deeply anesthetized with pentobarbital and
673 transcardially perfused with ice-cold 4% paraformaldehyde (PFA) in PBS. Brains were extracted
674 and fixed in 4% PFA for 4 h at 4 °C. The brains were equilibrated in 20% sucrose in PBS at 4 °C
675 overnight. Axial sections (40 μm) were prepared on a freezing microtome (model 860, AO
676 Scientific Instruments). Consecutive sections (120 μm apart) were mounted and examined with a
677 laser confocal microscope (Carl Zeiss LSM780). For immunohistochemistry, free-floating
678 sections were processed with 5% normal goat serum and 0.3% Triton X-100 in PBS with primary
679 antibodies against rabbit polyclonal to CaMKIIα (1:400; Abcam) and guinea pig polyclonal to
680 GABA (1:200; Abcam) at 4 °C for 24 h. After washing with PBS, sections were then incubated
681 for 2 h at room temperature with secondary antibodies Alexa Fluor 647 conjugate goat anti-rabbit
682 IgG and Alexa Fluor 488 conjugate goat anti-guinea pig IgG (both 1:500; Molecular Probe). Slices
683 were then washed and mounted using FluoroShield mounting medium with DAPI (Abcam).
684 Double or triple immunofluorescence was assessed with a laser confocal microscope (Carl Zeiss
685 LSM780).

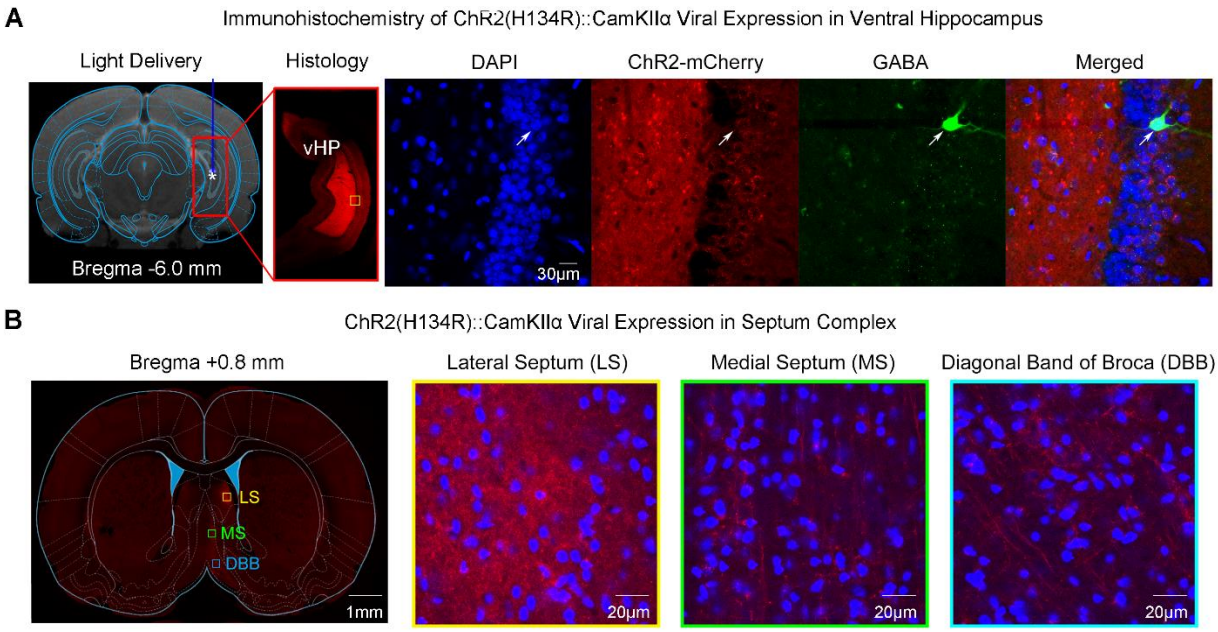

686

687 **Supplementary Figure 1. Histological characterization of ChR2::CaMKIIα viral expression in**
688 **ventral hippocampus (vHP) excitatory neurons demonstrates no colocalization with vHP GABAergic**
689 **neurons and their projection targets to the septum complex.** ***(A)*** Confocal images of ChR2-mCherry
690 expression in vHP; Lower magnification (*Left*) and higher magnification (*Right*). Overlay of images co-
691 stained for the nuclear marker DAPI, mCherry, and inhibitory marker GABA revealed no colocalization
692 between mCherry and vHP GABAergic neurons (indicated by white arrow). The yellow box indicates the
693 location of magnified confocal images shown in *B*. ***(B)*** Confocal images of ChR2-mCherry expression in
694 the septum complex. Lower magnification *(Left)* and higher magnification (*Right*). vHP projections synapse
695 in the Lateral Septum (LS), Medial Septum (MS), and Diagonal Band of Broca (DBB), indicated by no
696 colocalization between mCherry and DAPI.

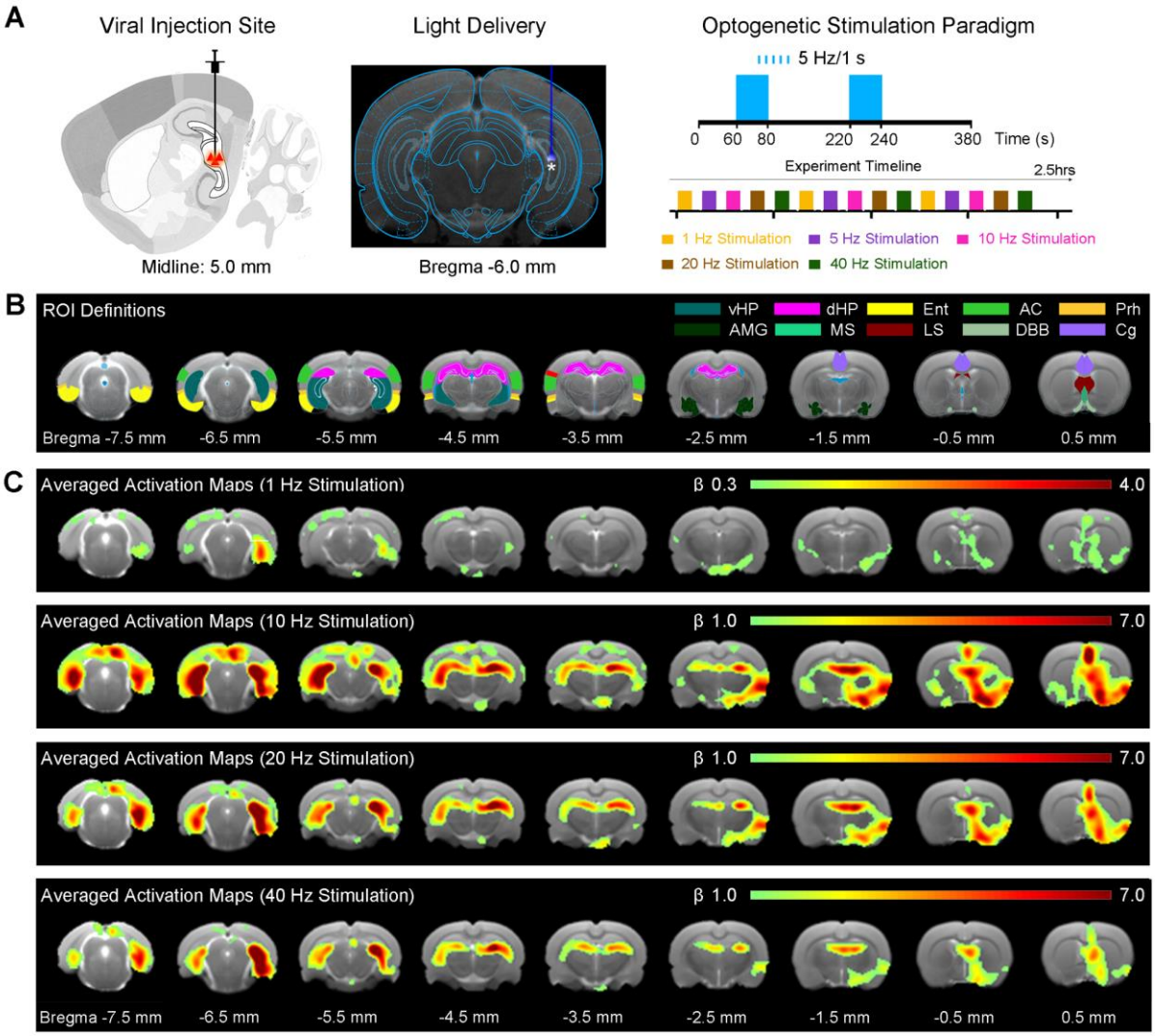

Supplementary Figure 2. Brain-wide activations detected in the hippocampal formation, cortical and subcortical regions during optogenetic stimulation of excitatory neurons in vHP. ***(A)*** Schematic *(Left)* and T2-weighted anatomical image *(Middle)* shows the viral injection and fiber implantation sites, respectively. Optogenetic fMRI stimulation paradigm *(Right)*. Optogenetic stimulations were presented in a block-design paradigm (20 seconds ON; 140 seconds OFF). Five frequencies (1, 5, 10, 20, 40 Hz) were interleaved by trials. ***(B)*** Regions of interest (ROIs) defined by the rat brain atlas to extract the BOLD signal profiles. ***(C)*** Averaged activation (β) maps of optogenetic stimulation of vHP excitatory neurons at 1, 10, 20, 40 Hz. Robust positive BOLD responses detected in bilateral vHP, dHP, Ent, AC, Prh, AMG, MS, LS, DBB, and Cg during 5 Hz optogenetic stimulation. Other frequencies (1 Hz, 10 Hz, 20 Hz, 40 Hz) evoked

707 weaker BOLD responses in Prh, MS, LS, and Cg, while retained strong BOLD responses in vHP and dHP.

708 ($n = 6$; $t > 3.1$, corresponding to $p < 0.001$).

709 Abbreviations: Ventral Hippocampus (vHP); Dorsal Hippocampus (dHP); Entorhinal Cortex (Ent);

710 Auditory Cortex (AC); Perirhinal Cortex (Prh); Amygdala (AMG); Medial Septum (MS); Lateral Septum

711 (LS); Diagonal Band of Broca (DBB); Cingulate Cortex (Cg).

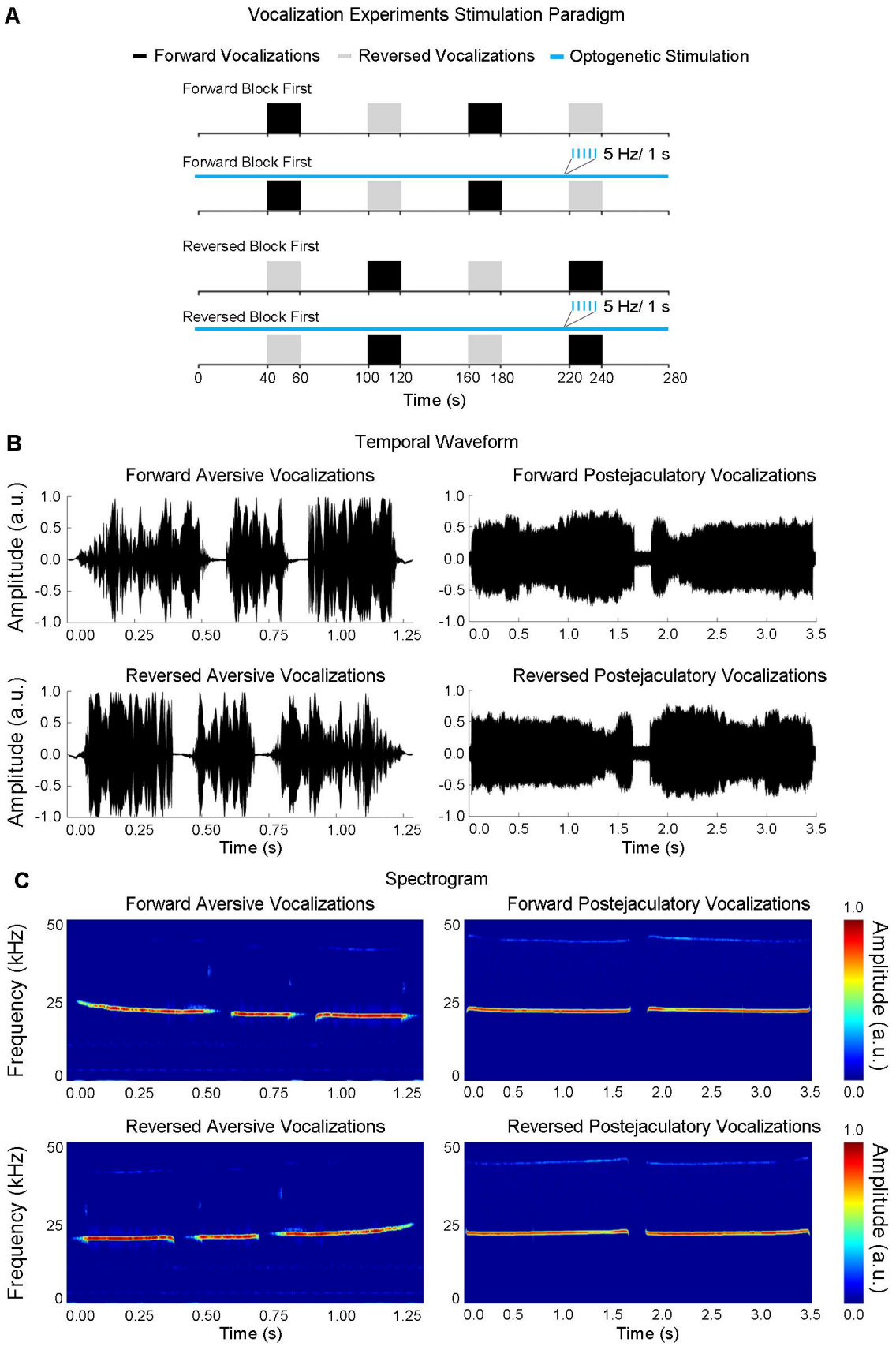

712

Supplementary Figure 3. Auditory and optogenetic stimulation paradigms for the negative/aversive and positive/postejaculatory vocalizations experiments. ***(A)*** The standard block paradigm (20 seconds ON and 40 seconds OFF) was used to present rat vocalizations to the left ear. Forward and reversed vocalizations were interleaved during each auditory fMRI session. The paradigm was repeated six times for each animal, with the first block occupied by forward and reversed vocalization each three times, while continuous 5 Hz optogenetic stimulation was alternating between auditory fMRI sessions. ***(B)*** The temporal waveforms of forward *(top left)* and temporally reversed *(bottom left)* aversive vocalizations and forward *(top right)* and temporally reversed *(bottom right)* postejaculatory vocalizations. ***(C)*** The spectrograms of forward *(top left)* and temporally reversed *(bottom left)* aversive vocalizations and forward *(top right)* and temporally reversed *(bottom right)* postejaculatory vocalizations.

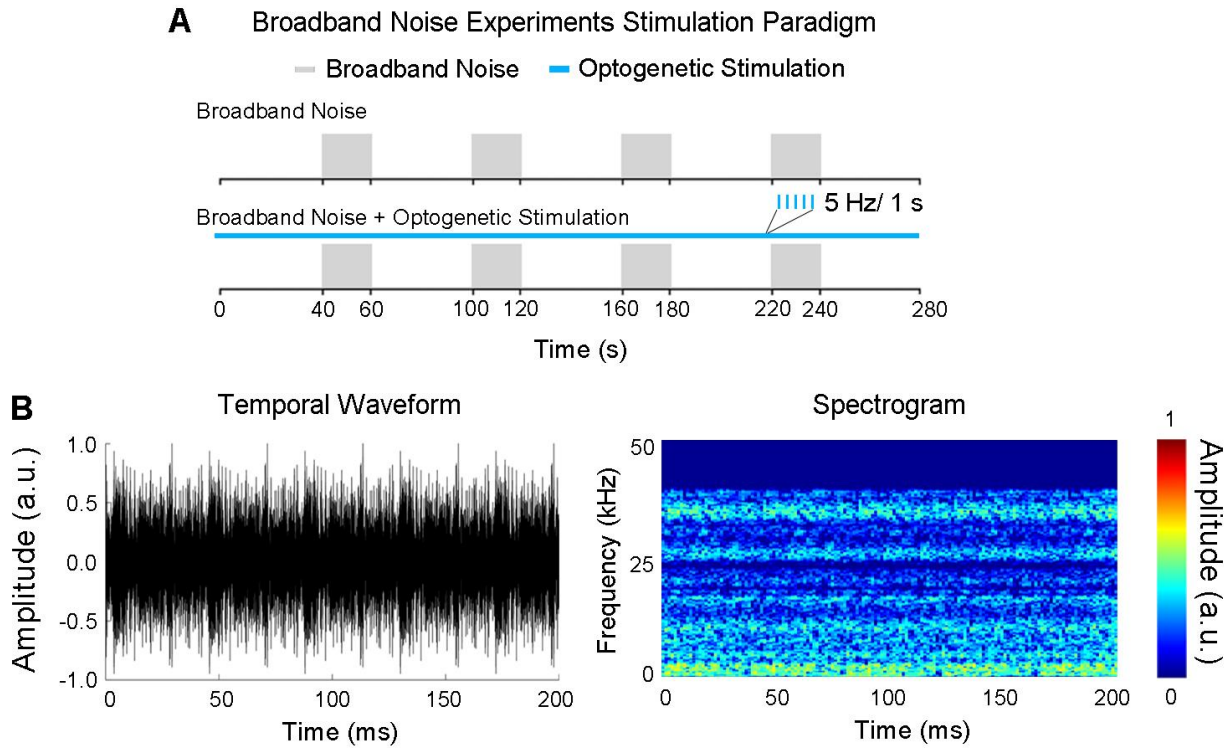

723

724 **Supplementary Figure 4. Auditory and optogenetic stimulation paradigms for broadband acoustic**
725 **noise experiments.** ***(A)*** The standard block paradigm (20 seconds ON and 40 seconds OFF) used to present
726 broadband noise to the left ear, while continuous 5 Hz optogenetic stimulation was alternating between
727 auditory fMRI sessions. ***(B)*** The temporal waveforms of the broadband noise. ***(C)*** The spectrograms of the
728 broadband noise.

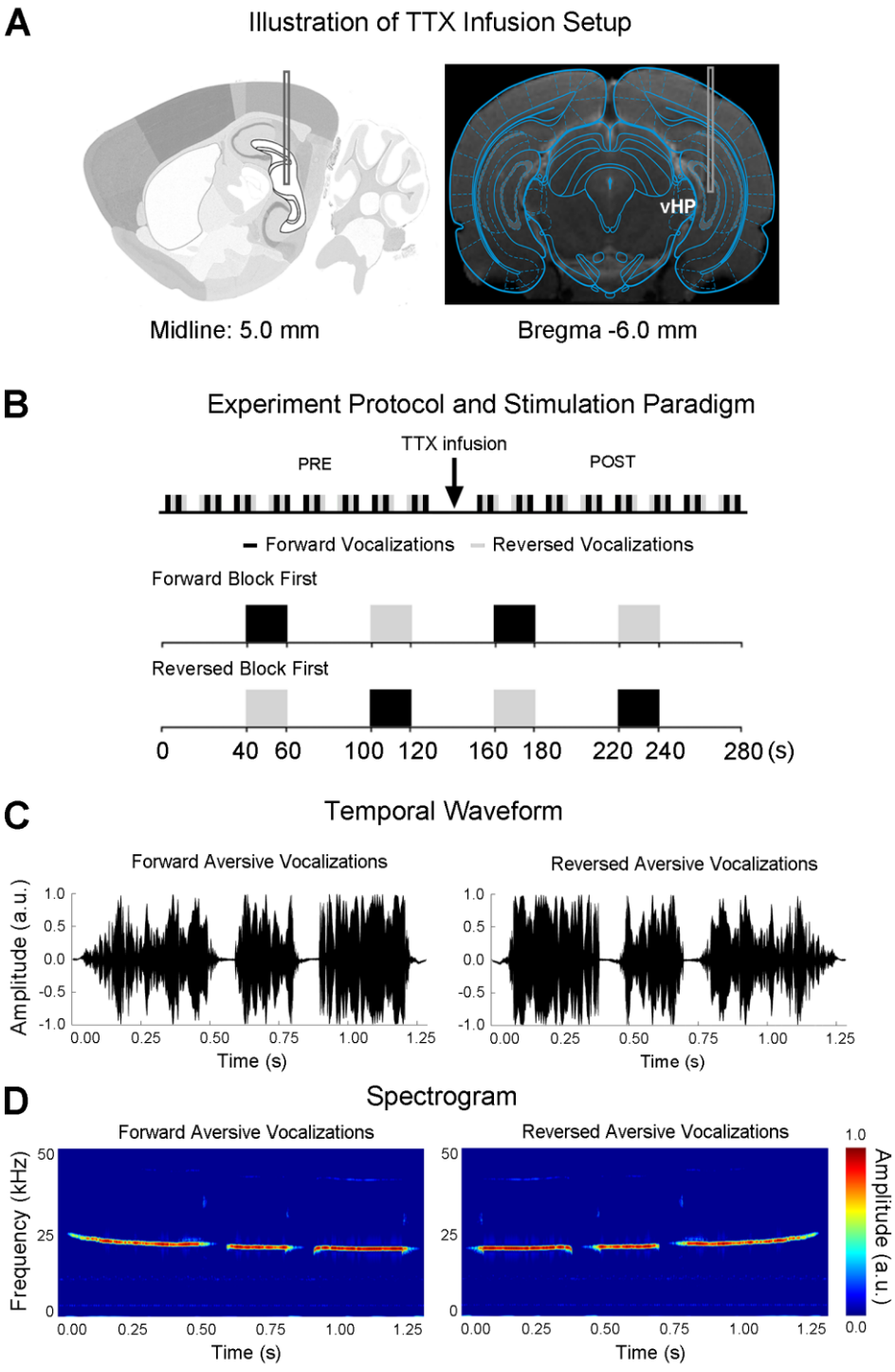

729

730 **Supplementary Figure 5. Illustration of tetrodotoxin (TTX) infusion to vHP, and corresponding**
731 **auditory fMRI stimulation paradigm for the negative/aversive vocalization experiments.** ***(A)*** TTX was
732 infused to the vHP with an implanted cannula. ***(B)*** Sixteen fMRI sessions were typically acquired during

an experiment. TTX was infused after eight fMRI sessions. Standard block design paradigm (20 seconds ON and 40 seconds OFF) was used to present vocalizations to the left ear. Forward and reversed vocalizations were interleaved during each auditory fMRI session. ***(C)*** The temporal waveform of forward *(left)* and temporally reversed *(right)* aversive vocalizations. ***(D)*** The spectrograms of forward *(left)* and temporally reversed *(right)* aversive vocalizations.

References

1. A. A. Sitko, L. V. Goodrich, Making sense of neural development by comparing wiring strategies for seeing and hearing. *Science* **371** (2021).
2. C. Schreiner, J. A. Winer, *The inferior colliculus* (Springer, 2005).
3. M. S. Malmierca, "Auditory system" in The rat nervous system. (Elsevier, 2015), pp. 865-946.
4. G. Chechik *et al.*, Reduction of information redundancy in the ascending auditory pathway. *Neuron* **51**, 359-368 (2006).
5. A. M. Leaver, J. P. Rauschecker, Cortical representation of natural complex sounds: effects of acoustic features and auditory object category. *J Neurosci* **30**, 7604-7612 (2010).
6. J. J. Eggermont, Between sound and perception: reviewing the search for a neural code. *Hear Res* **157**, 1-42 (2001).
7. N. Suga, X. Ma, Multiparametric corticofugal modulation and plasticity in the auditory system. *Nat Rev Neurosci* **4**, 783-794 (2003).
8. G. Kim, A. Doupe, Organized representation of spectrotemporal features in songbird auditory forebrain. *J Neurosci* **31**, 16977-16990 (2011).
9. M. Ono, D. C. Bishop, D. L. Oliver, Identified GABAergic and Glutamatergic Neurons in the Mouse Inferior Colliculus Share Similar Response Properties. *J Neurosci* **37**, 8952-8964 (2017).
10. J. Sturm, T. Nguyen, K. Kandler, Development of intrinsic connectivity in the central nucleus of the mouse inferior colliculus. *J Neurosci* **34**, 15032-15046 (2014).
11. K. I. Nagel, A. J. Doupe, Organizing principles of spectro-temporal encoding in the avian primary auditory area field L. *Neuron* **58**, 938-955 (2008).
12. D. M. Schneider, S. M. Woolley, Extra-classical tuning predicts stimulus-dependent receptive fields in auditory neurons. *J Neurosci* **31**, 11867-11878 (2011).
13. S. M. Woolley, P. R. Gill, F. E. Theunissen, Stimulus-dependent auditory tuning results in synchronous population coding of vocalizations in the songbird midbrain. *J Neurosci* **26**, 2499-2512 (2006).
14. C. V. Portfors, Types and functions of ultrasonic vocalizations in laboratory rats and mice. *J Am Assoc Lab Anim Sci* **46**, 28-34 (2007).
15. S. M. Woolley, C. V. Portfors, Conserved mechanisms of vocalization coding in mammalian and songbird auditory midbrain. *Hear Res* **305**, 45-56 (2013).
16. A. M. Simmons, "Perspectives and progress in animal acoustic communication" in Acoustic communication. (Springer, 2003), pp. 1-14.
17. F. E. Theunissen, J. E. Elie, Neural processing of natural sounds. *Nat Rev Neurosci* **15**, 355-366 (2014).
18. T. Overath, J. H. McDermott, J. M. Zarate, D. Poeppel, The cortical analysis of speech-specific temporal structure revealed by responses to sound quilts. *Nat Neurosci* **18**, 903-911 (2015).
19. G. W. Zhang *et al.*, A Non-canonical Reticular-Limbic Central Auditory Pathway via Medial Septum Contributes to Fear Conditioning. *Neuron* **97**, 406-417 e404 (2018).
20. D. Aronov, R. Nevers, D. W. Tank, Mapping of a non-spatial dimension by the hippocampal-entorhinal circuit. *Nature* **543**, 719-722 (2017).
21. W. Guo, B. Robert, D. B. Polley, The Cholinergic Basal Forebrain Links Auditory Stimuli with Delayed Reinforcement to Support Learning. *Neuron* **103**, 1164-1177 e1166 (2019).
22. C. Xiao, Y. Liu, J. Xu, X. Gan, Z. Xiao, Septal and Hippocampal Neurons Contribute to Auditory Relay and Fear Conditioning. *Front Cell Neurosci* **12**, 102 (2018).
23. J. A. Winer, Decoding the auditory corticofugal systems. *Hear Res* **212**, 1-8 (2006).
24. X. R. Xiong *et al.*, Auditory cortex controls sound-driven innate defense behaviour through corticofugal projections to inferior colliculus. *Nat Commun* **6**, 7224 (2015).
25. J. M. Blackwell, A. M. Lesicko, W. Rao, M. De Biasi, M. N. Geffen, Auditory cortex shapes sound responses in the inferior colliculus. *Elife* **9** (2020).

26. A. M. H. Lesicko, S. K. Sons, D. A. Llano, Circuit Mechanisms Underlying the Segregation and Integration of Parallel Processing Streams in the Inferior Colliculus. *J Neurosci* **40**, 6328-6344 (2020).
27. L. Chen, X. Wang, S. Ge, Q. Xiong, Medial geniculate body and primary auditory cortex differentially contribute to striatal sound representations. *Nat Commun* **10**, 418 (2019).
28. B. M. J. Olthof, A. Rees, S. E. Gartside, Multiple Nonauditory Cortical Regions Innervate the Auditory Midbrain. *J Neurosci* **39**, 8916-8928 (2019).
29. R. A. Marsh, Z. M. Fuzessery, C. D. Grose, J. J. Wenstrup, Projection to the inferior colliculus from the basal nucleus of the amygdala. *J Neurosci* **22**, 10449-10460 (2002).
30. C. M. Bird, N. Burgess, The hippocampus and memory: insights from spatial processing. *Nat Rev Neurosci* **9**, 182-194 (2008).
31. G. Buzsaki, E. I. Moser, Memory, navigation and theta rhythm in the hippocampal-entorhinal system. *Nat Neurosci* **16**, 130-138 (2013).
32. J. Lisman *et al.*, Viewpoints: how the hippocampus contributes to memory, navigation and cognition. *Nat Neurosci* **20**, 1434-1447 (2017).
33. D. Aronov, R. Nevers, D. W. Tank, Mapping of a non-spatial dimension by the hippocampal-entorhinal circuit. *Nature* **543**, 719-722 (2017).
34. S. Terada, Y. Sakurai, H. Nakahara, S. Fujisawa, Temporal and Rate Coding for Discrete Event Sequences in the Hippocampus. *Neuron* **94**, 1248-1262 e1244 (2017).
35. D. Bendor, M. A. Wilson, Biasing the content of hippocampal replay during sleep. *Nat Neurosci* **15**, 1439-1444 (2012).
36. G. Rothschild, E. Eban, L. M. Frank, A cortical-hippocampal-cortical loop of information processing during memory consolidation. *Nat Neurosci* **20**, 251-259 (2017).
37. G. Buzsaki, The hippocampo-neocortical dialogue. *Cereb Cortex* **6**, 81-92 (1996).
38. N. M. van Strien, N. L. Cappaert, M. P. Witter, The anatomy of memory: an interactive overview of the parahippocampal-hippocampal network. *Nat Rev Neurosci* **10**, 272-282 (2009).
39. S. W. Oh *et al.*, A mesoscale connectome of the mouse brain. *Nature* **508**, 207-214 (2014).
40. M. M. Munoz-Lopez, A. Mohedano-Moriano, R. Insausti, Anatomical pathways for auditory memory in primates. *Front Neuroanat* **4**, 129 (2010).
41. L. A. Cenquizca, L. W. Swanson, Spatial organization of direct hippocampal field CA1 axonal projections to the rest of the cerebral cortex. *Brain Res Rev* **56**, 1-26 (2007).
42. M. S. Fanselow, H. W. Dong, Are the dorsal and ventral hippocampus functionally distinct structures? *Neuron* **65**, 7-19 (2010).
43. B. A. Strange, M. P. Witter, E. S. Lein, E. I. Moser, Functional organization of the hippocampal longitudinal axis. *Nat Rev Neurosci* **15**, 655-669 (2014).
44. E. V. Lubenov, A. G. Siapas, Hippocampal theta oscillations are travelling waves. *Nature* **459**, 534-539 (2009).
45. J. Patel, S. Fujisawa, A. Berenyi, S. Royer, G. Buzsaki, Traveling theta waves along the entire septotemporal axis of the hippocampus. *Neuron* **75**, 410-417 (2012).
46. P. P. Gao, J. W. Zhang, S. J. Fan, D. H. Sanes, E. X. Wu, Auditory midbrain processing is differentially modulated by auditory and visual cortices: An auditory fMRI study. *Neuroimage* **123**, 22-32 (2015).
47. M. M. Asokan, R. S. Williamson, K. E. Hancock, D. B. Polley, Sensory overamplification in layer 5 auditory corticofugal projection neurons following cochlear nerve synaptic damage. *Nat Commun* **9**, 2468 (2018).
48. J. P. Rauschecker, S. K. Scott, Maps and streams in the auditory cortex: nonhuman primates illuminate human speech processing. *Nat Neurosci* **12**, 718-724 (2009).
49. J. P. Rauschecker, B. Tian, Mechanisms and streams for processing of "what" and "where" in auditory cortex. *Proc Natl Acad Sci U S A* **97**, 11800-11806 (2000).
50. W. Guo, A. R. Clause, A. Barth-Maron, D. B. Polley, A Corticothalamic Circuit for Dynamic Switching between Feature Detection and Discrimination. *Neuron* **95**, 180-194 e185 (2017).

51. P. G. Mihai *et al.*, Modulation of tonotopic ventral medial geniculate body is behaviorally relevant for speech recognition. *Elife* **8** (2019).
52. B. Diaz, F. Hintz, S. J. Kiebel, K. von Kriegstein, Dysfunction of the auditory thalamus in developmental dyslexia. *Proc Natl Acad Sci U S A* **109**, 13841-13846 (2012).
53. R. A. Felix, 2nd, B. Gourevitch, C. V. Portfors, Subcortical pathways: Towards a better understanding of auditory disorders. *Hear Res* **362**, 48-60 (2018).
54. J. A. Winer, C. E. Schreiner, "The central auditory system: a functional analysis" in The inferior colliculus. (Springer, 2005), pp. 1-68.
55. G. D. Pollak, The dominant role of inhibition in creating response selectivities for communication calls in the brainstem auditory system. *Hear Res* **305**, 86-101 (2013).
56. S. M. Woolley, C. V. Portfors, Conserved mechanisms of vocalization coding in mammalian and songbird auditory midbrain. *Hear Res* **305**, 45-56 (2013).
57. C. Muller, S. Remy, Septo-hippocampal interaction. *Cell Tissue Res* **373**, 565-575 (2018).
58. M. F. Yeckel, T. W. Berger, Feedforward excitation of the hippocampus by afferents from the entorhinal cortex: redefinition of the role of the trisynaptic pathway. *Proc Natl Acad Sci U S A* **87**, 5832-5836 (1990).
59. Y. Yang *et al.*, Opposite monosynaptic scaling of BLP-vCA1 inputs governs hopefulness- and helplessness-modulated spatial learning and memory. *Nat Commun* **7**, 11935 (2016).
60. A. C. Felix-Ortiz, K. M. Tye, Amygdala inputs to the ventral hippocampus bidirectionally modulate social behavior. *J Neurosci* **34**, 586-595 (2014).
61. P. H. Janak, K. M. Tye, From circuits to behaviour in the amygdala. *Nature* **517**, 284-292 (2015).
62. A. R. Preston, H. Eichenbaum, Interplay of hippocampus and prefrontal cortex in memory. *Curr Biol* **23**, R764-773 (2013).
63. E. T. Rolls, Limbic systems for emotion and for memory, but no single limbic system. *Cortex* **62**, 119-157 (2015).
64. D. H. Lindquist, L. E. Jarrard, T. H. Brown, Perirhinal cortex supports delay fear conditioning to rat ultrasonic social signals. *J Neurosci* **24**, 3610-3617 (2004).
65. D. Yaniv, A. Desmedt, R. Jaffard, G. Richter-Levin, The amygdala and appraisal processes: stimulus and response complexity as an organizing factor. *Brain Res Brain Res Rev* **44**, 179-186 (2004).
66. R. S. Williamson, D. B. Polley, Parallel pathways for sound processing and functional connectivity among layer 5 and 6 auditory corticofugal neurons. *Elife* **8** (2019).
67. N. Y. Homma *et al.*, A Role for Auditory Corticothalamic Feedback in the Perception of Complex Sounds. *J Neurosci* **37**, 6149-6161 (2017).
68. T. Donishi, A. Kimura, H. Imbe, I. Yokoi, Y. Kaneoke, Sub-threshold cross-modal sensory interaction in the thalamus: lemniscal auditory response in the medial geniculate nucleus is modulated by somatosensory stimulation. *Neuroscience* **174**, 200-215 (2011).
69. G. Corder *et al.*, An amygdalar neural ensemble that encodes the unpleasantness of pain. *Science* **363**, 276-281 (2019).
70. A. Singh *et al.*, Mapping Cortical Integration of Sensory and Affective Pain Pathways. *Curr Biol* **30**, 1703-1715 e1705 (2020).
71. K. M. Barry, D. Robertson, W. Mulders, Medial geniculate neurons show diverse effects in response to electrical stimulation of prefrontal cortex. *Hear Res* **353**, 204-212 (2017).
72. X. J. Yu, X. X. Xu, S. He, J. He, Change detection by thalamic reticular neurons. *Nat Neurosci* **12**, 1165-1170 (2009).
73. M. Aizenberg *et al.*, Projection from the Amygdala to the Thalamic Reticular Nucleus Amplifies Cortical Sound Responses. *Cell Rep* **28**, 605-615 e604 (2019).
74. A. Poremba, M. Gabriel, Amygdalar efferents initiate auditory thalamic discriminative training-induced neuronal activity. *J Neurosci* **21**, 270-278 (2001).
75. S. O'Mara, The subiculum: what it does, what it might do, and what neuroanatomy has yet to tell us. *J Anat* **207**, 271-282 (2005).

76. L. R. Squire, H. Schmolck, S. M. Stark, Impaired auditory recognition memory in amnesic patients with medial temporal lobe lesions. *Learn Mem* **8**, 252-256 (2001).
77. J. Plailly, B. Tillmann, J. P. Royet, The feeling of familiarity of music and odors: the same neural signature? *Cereb Cortex* **17**, 2650-2658 (2007).
78. G. Vega-Flores *et al.*, The GABAergic septohippocampal pathway is directly involved in internal processes related to operant reward learning. *Cereb Cortex* **24**, 2093-2107 (2014).
79. I. Klinkenberg, A. Blokland, The validity of scopolamine as a pharmacological model for cognitive impairment: a review of animal behavioral studies. *Neurosci Biobehav Rev* **34**, 1307-1350 (2010).
80. C. Chavez, L. Zaborszky, Basal Forebrain Cholinergic-Auditory Cortical Network: Primary Versus Nonprimary Auditory Cortical Areas. *Cereb Cortex* **27**, 2335-2347 (2017).
81. N. C. Tronson *et al.*, Segregated populations of hippocampal principal CA1 neurons mediating conditioning and extinction of contextual fear. *J Neurosci* **29**, 3387-3394 (2009).
82. H. J. Gritton *et al.*, Cortical cholinergic signaling controls the detection of cues. *Proc Natl Acad Sci U S A* **113**, E1089-1097 (2016).
83. J. J. Roland *et al.*, Medial septum-diagonal band of Broca (MSDB) GABAergic regulation of hippocampal acetylcholine efflux is dependent on cognitive demands. *J Neurosci* **34**, 506-514 (2014).
84. J. M. Staib, R. Della Valle, D. K. Knox, Disruption of medial septum and diagonal bands of Broca cholinergic projections to the ventral hippocampus disrupt auditory fear memory. *Neurobiol Learn Mem* **152**, 71-79 (2018).
85. A. Nelson, R. Mooney, The Basal Forebrain and Motor Cortex Provide Convergent yet Distinct Movement-Related Inputs to the Auditory Cortex. *Neuron* **90**, 635-648 (2016).
86. L. Jiang *et al.*, Cholinergic Signaling Controls Conditioned Fear Behaviors and Enhances Plasticity of Cortical-Amygdala Circuits. *Neuron* **90**, 1057-1070 (2016).
87. M. Siegel, K. P. Kording, P. Konig, Integrating top-down and bottom-up sensory processing by somato-dendritic interactions. *J Comput Neurosci* **8**, 161-173 (2000).
88. A. K. Engel, P. Fries, W. Singer, Dynamic predictions: oscillations and synchrony in top-down processing. *Nat Rev Neurosci* **2**, 704-716 (2001).
89. R. Mooney, The neurobiology of innate and learned vocalizations in rodents and songbirds. *Curr Opin Neurobiol* **64**, 24-31 (2020).
90. E. J. Mahrt, D. J. Perkel, L. Tong, E. W. Rubel, C. V. Portfors, Engineered deafness reveals that mouse courtship vocalizations do not require auditory experience. *J Neurosci* **33**, 5573-5583 (2013).
91. M. Bialy, W. Bogacki-Rychlik, K. Kasarello, E. Nikolaev, E. M. Sajdel-Sulkowska, Modulation of 22-khz postejaculatory vocalizations by conditioning to new place: Evidence for expression of a positive emotional state. *Behav Neurosci* **130**, 415-421 (2016).
92. M. Bialy, M. Podobinska, J. Barski, W. Bogacki-Rychlik, E. M. Sajdel-Sulkowska, Distinct classes of low frequency ultrasonic vocalizations in rats during sexual interactions relate to different emotional states. *Acta Neurobiol Exp (Wars)* **79**, 1-12 (2019).
93. H. Eichenbaum, Time cells in the hippocampus: a new dimension for mapping memories. *Nat Rev Neurosci* **15**, 732-744 (2014).
94. R. P. Kesner, M. R. Hunsaker, P. E. Gilbert, The role of CA1 in the acquisition of an object-trace-odor paired associate task. *Behav Neurosci* **119**, 781-786 (2005).
95. L. M. DeVito *et al.*, Vasopressin 1b receptor knock-out impairs memory for temporal order. *J Neurosci* **29**, 2676-2683 (2009).
96. A. R. Mayes *et al.*, Memory for single items, word pairs, and temporal order of different kinds in a patient with selective hippocampal lesions. *Cogn Neuropsychol* **18**, 97-123 (2001).
97. H. J. Spiers, N. Burgess, T. Hartley, F. Vargha-Khadem, J. O'Keefe, Bilateral hippocampal pathology impairs topographical and episodic memory but not visual pattern matching. *Hippocampus* **11**, 715-725 (2001).

98. N. S. Jacobs, T. A. Allen, N. Nguyen, N. J. Fortin, Critical role of the hippocampus in memory for elapsed time. *J Neurosci* **33**, 13888-13893 (2013).
99. K. Z. Tanaka *et al.*, The hippocampal engram maps experience but not place. *Science* **361**, 392-397 (2018).
100. D. A. Ross, P. Sadil, D. M. Wilson, R. A. Cowell, Hippocampal Engagement during Recall Depends on Memory Content. *Cereb Cortex* **28**, 2685-2698 (2018).
101. L. M. Rangel *et al.*, Rhythmic coordination of hippocampal neurons during associative memory processing. *Elife* **5**, e09849 (2016).
102. D. B. Headley, D. Pare, Common oscillatory mechanisms across multiple memory systems. *NPJ Sci Learn* **2** (2017).
103. E. Nyhus, T. Curran, Functional role of gamma and theta oscillations in episodic memory. *Neurosci Biobehav Rev* **34**, 1023-1035 (2010).
104. P. B. Sederberg, M. J. Kahana, M. W. Howard, E. J. Donner, J. R. Madsen, Theta and gamma oscillations during encoding predict subsequent recall. *J Neurosci* **23**, 10809-10814 (2003).
105. G. Dragoi, Cell assemblies, sequences and temporal coding in the hippocampus. *Curr Opin Neurobiol* **64**, 111-118 (2020).
106. D. B. Headley, N. M. Weinberger, Fear conditioning enhances gamma oscillations and their entrainment of neurons representing the conditioned stimulus. *J Neurosci* **33**, 5705-5717 (2013).
107. L. L. Colgin, Rhythms of the hippocampal network. *Nat Rev Neurosci* **17**, 239-249 (2016).
108. M. J. Jutras, P. Fries, E. A. Buffalo, Oscillatory activity in the monkey hippocampus during visual exploration and memory formation. *Proc Natl Acad Sci U S A* **110**, 13144-13149 (2013).
109. G. Buzsaki, Theta rhythm of navigation: link between path integration and landmark navigation, episodic and semantic memory. *Hippocampus* **15**, 827-840 (2005).
110. A. Sirota *et al.*, Entrainment of neocortical neurons and gamma oscillations by the hippocampal theta rhythm. *Neuron* **60**, 683-697 (2008).
111. A. G. Siapas, E. V. Lubenov, M. A. Wilson, Prefrontal phase locking to hippocampal theta oscillations. *Neuron* **46**, 141-151 (2005).
112. J. J. Chrobak, G. Buzsaki, Gamma oscillations in the entorhinal cortex of the freely behaving rat. *J Neurosci* **18**, 388-398 (1998).
113. P. Telensky *et al.*, Functional inactivation of the rat hippocampus disrupts avoidance of a moving object. *Proc Natl Acad Sci U S A* **108**, 5414-5418 (2011).
114. R. W. Chan *et al.*, Low-frequency hippocampal-cortical activity drives brain-wide resting-state functional MRI connectivity. *Proc Natl Acad Sci U S A* **114**, E6972-E6981 (2017).
115. A. T. L. Leong *et al.*, Optogenetic auditory fMRI reveals the effects of visual cortical inputs on auditory midbrain response. *Sci Rep* **8**, 8736 (2018).

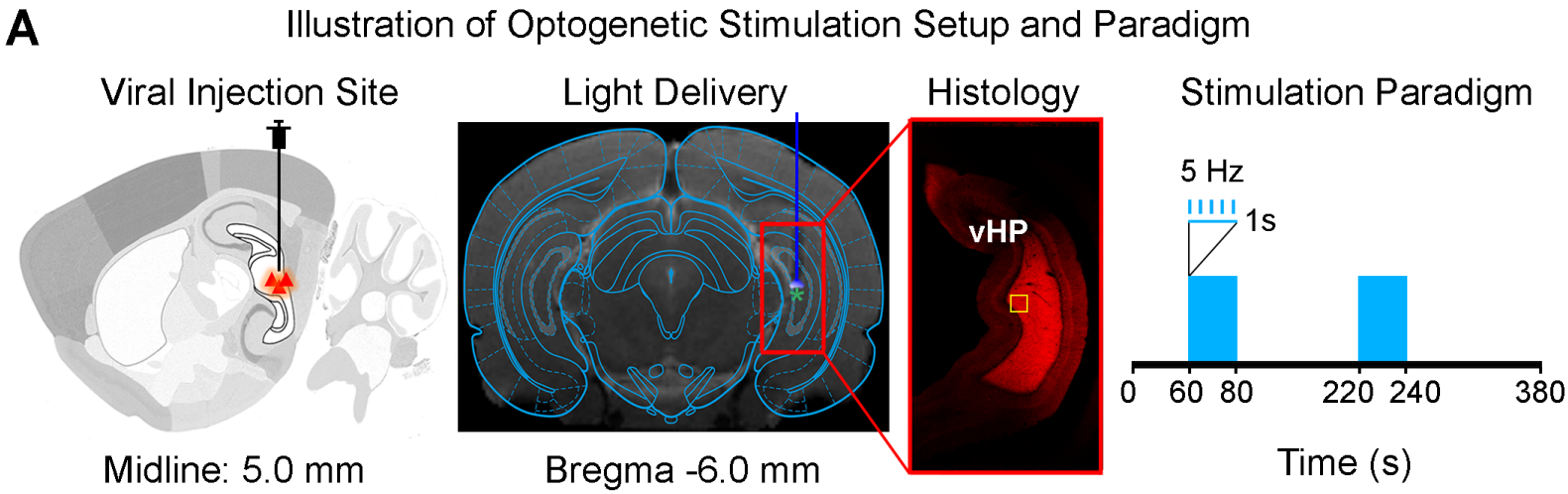

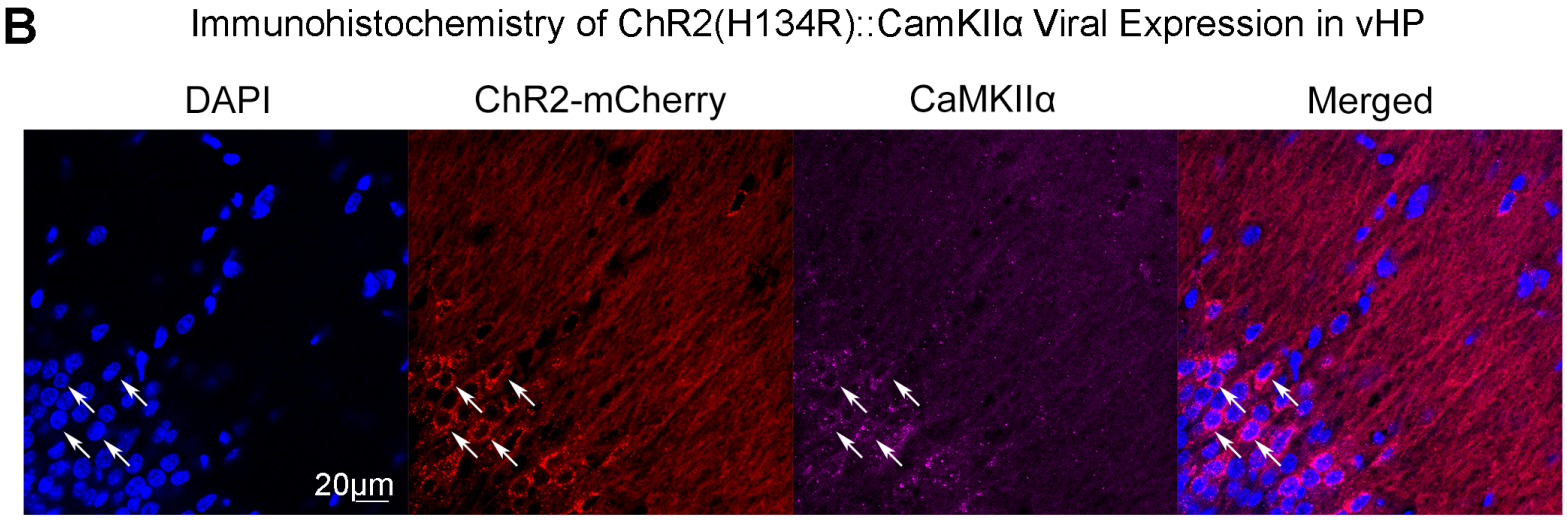

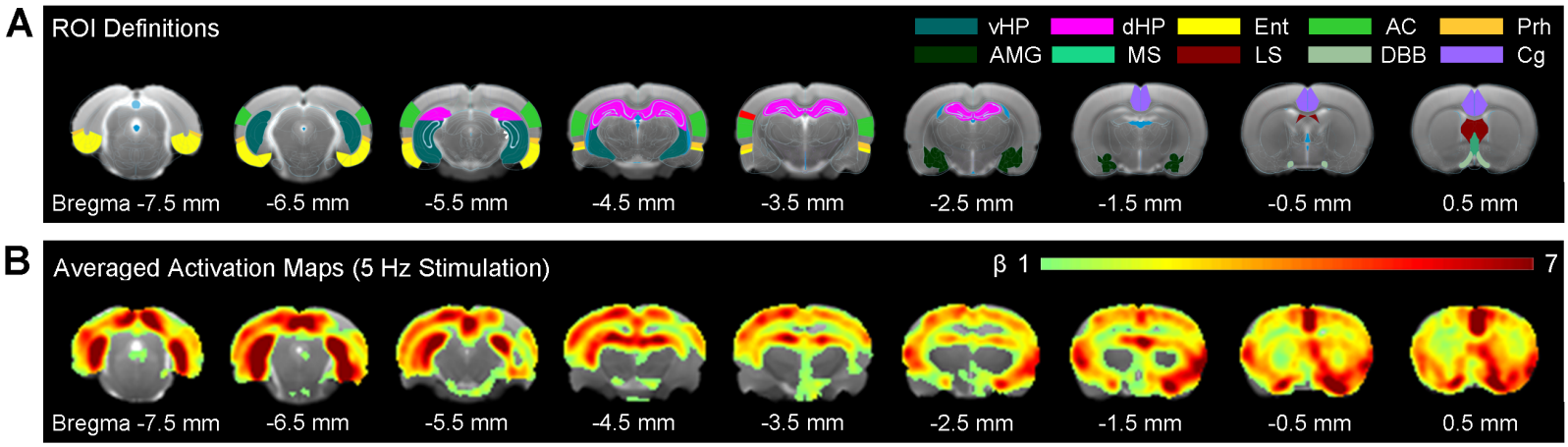

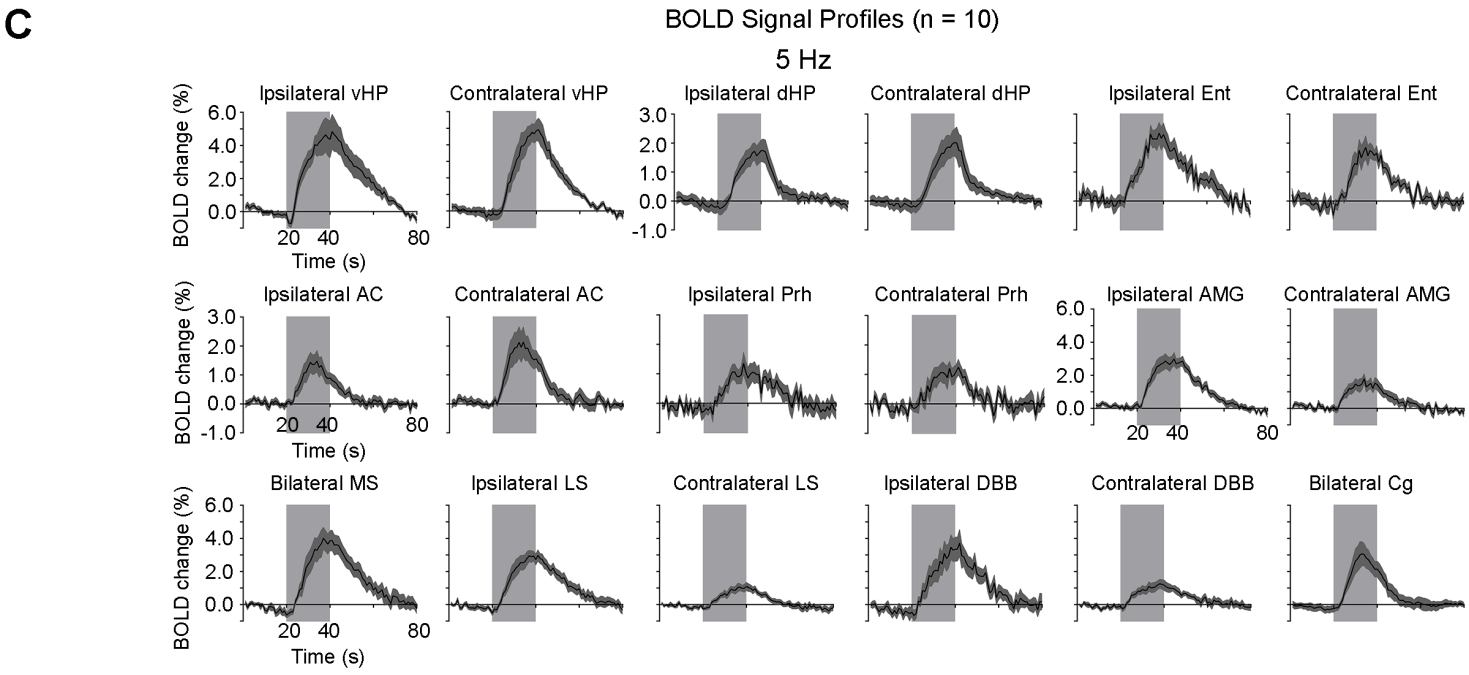

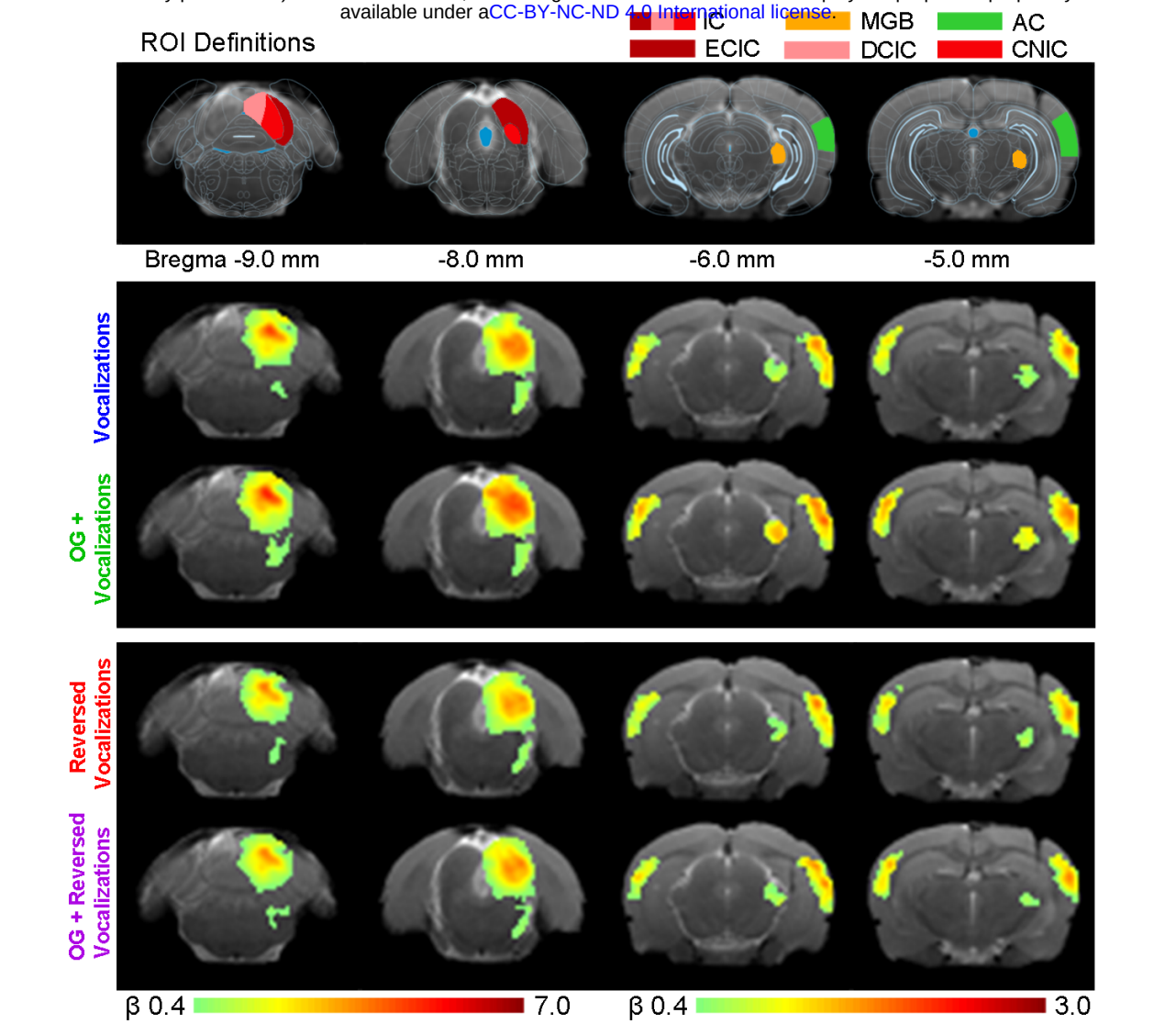

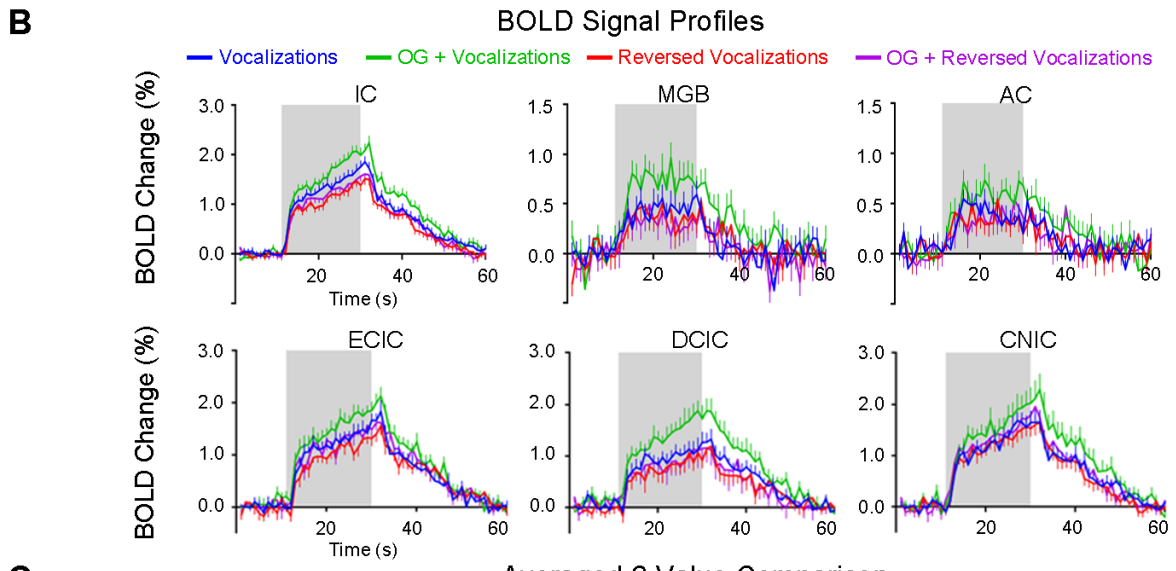

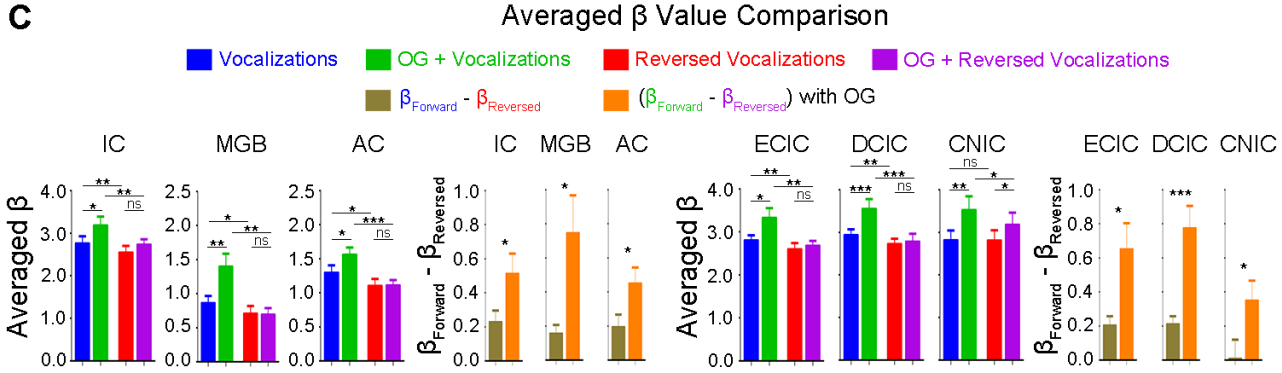

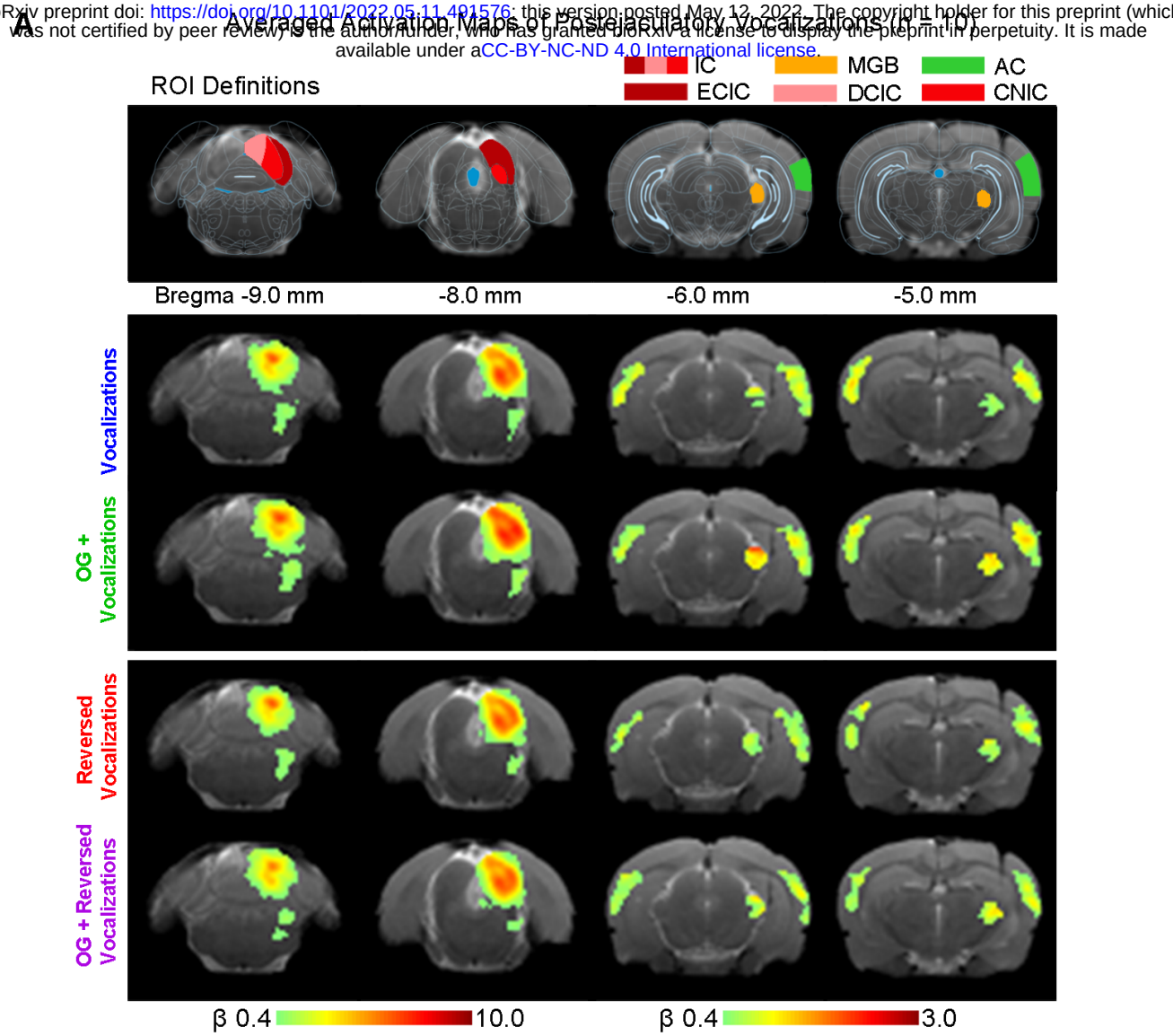

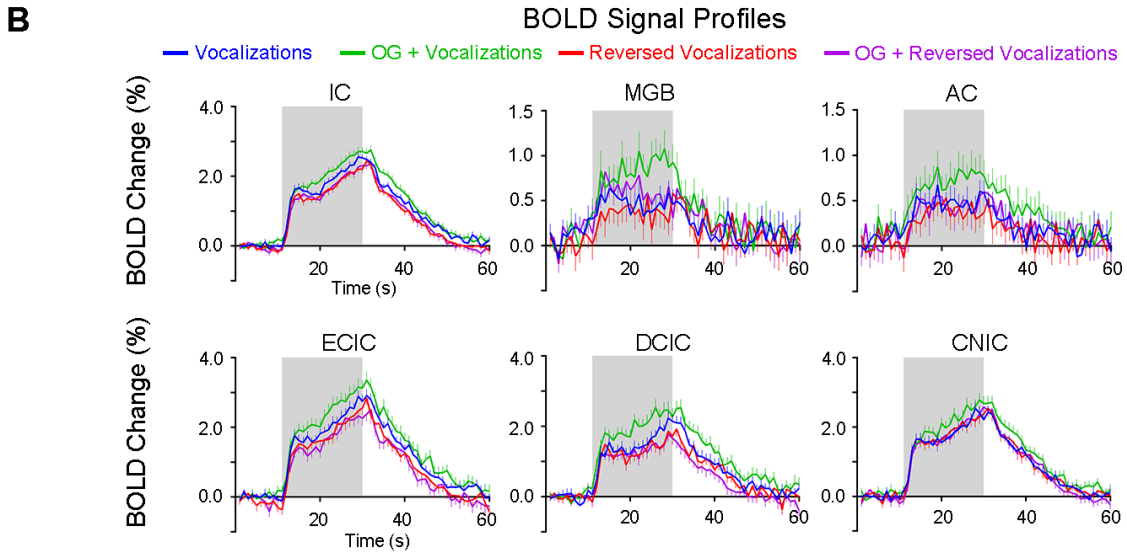

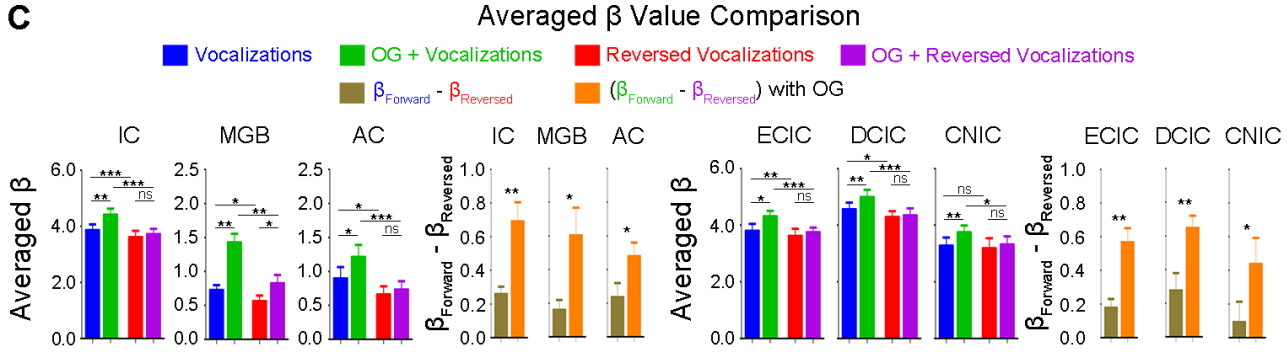

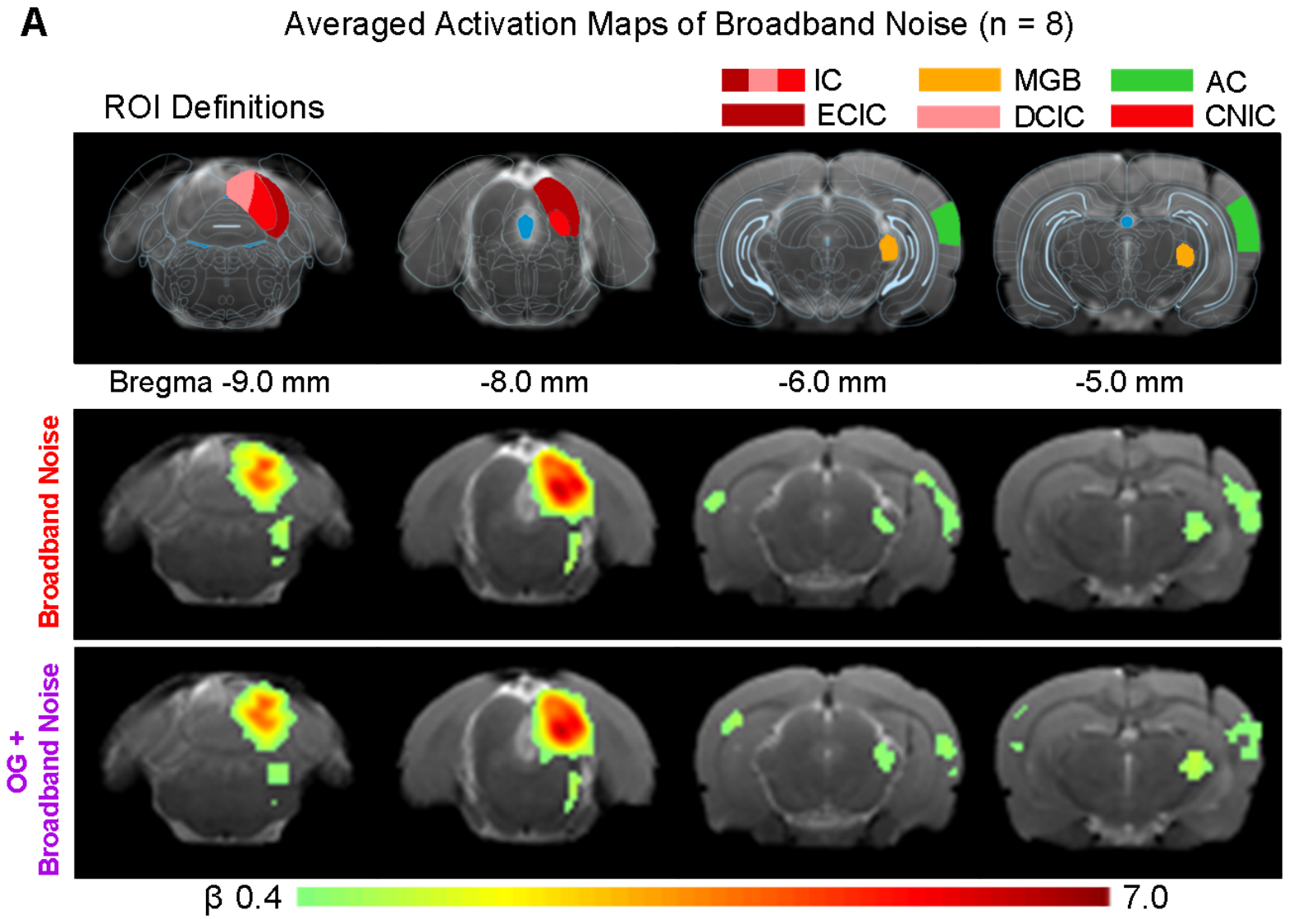

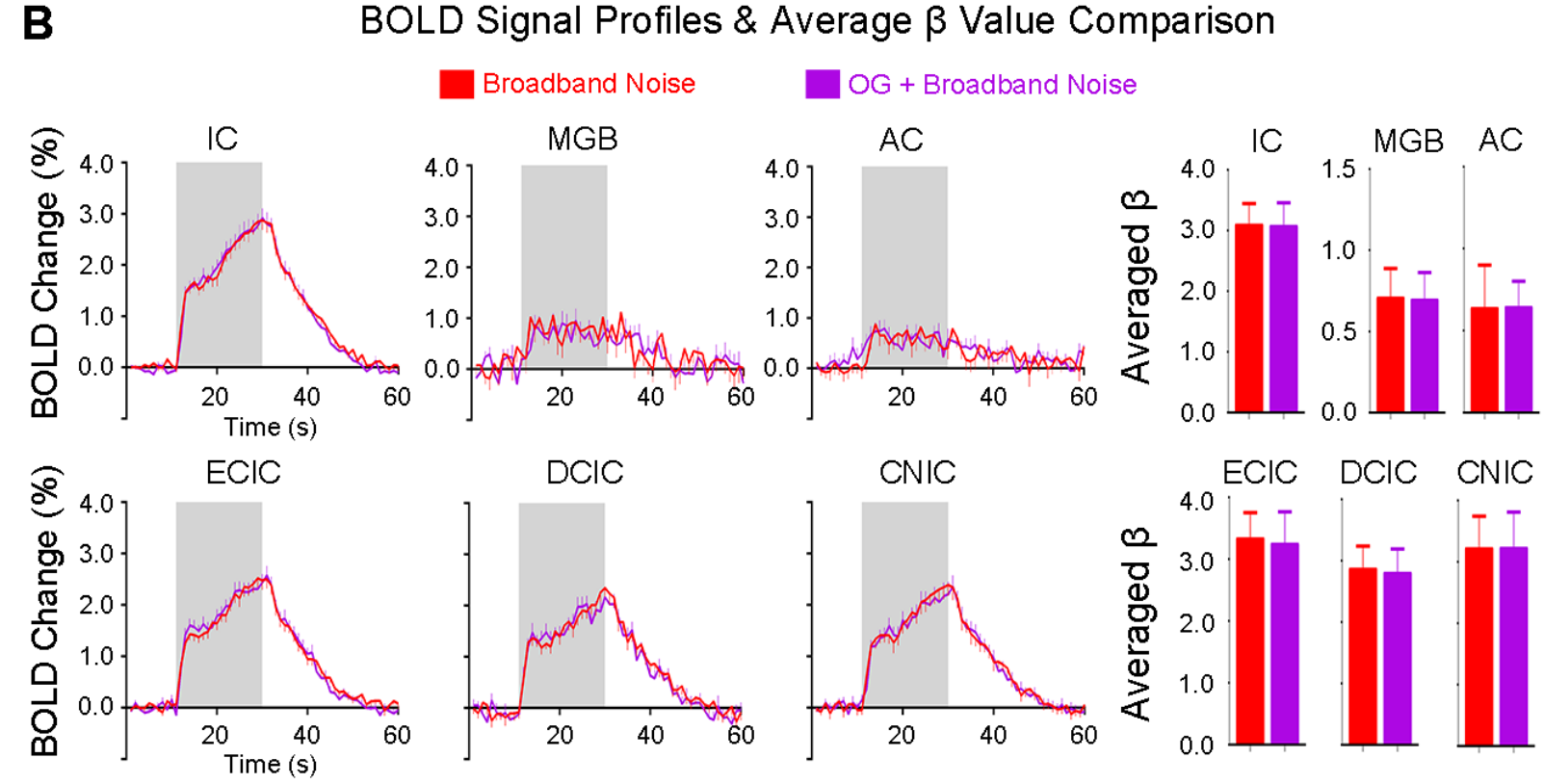

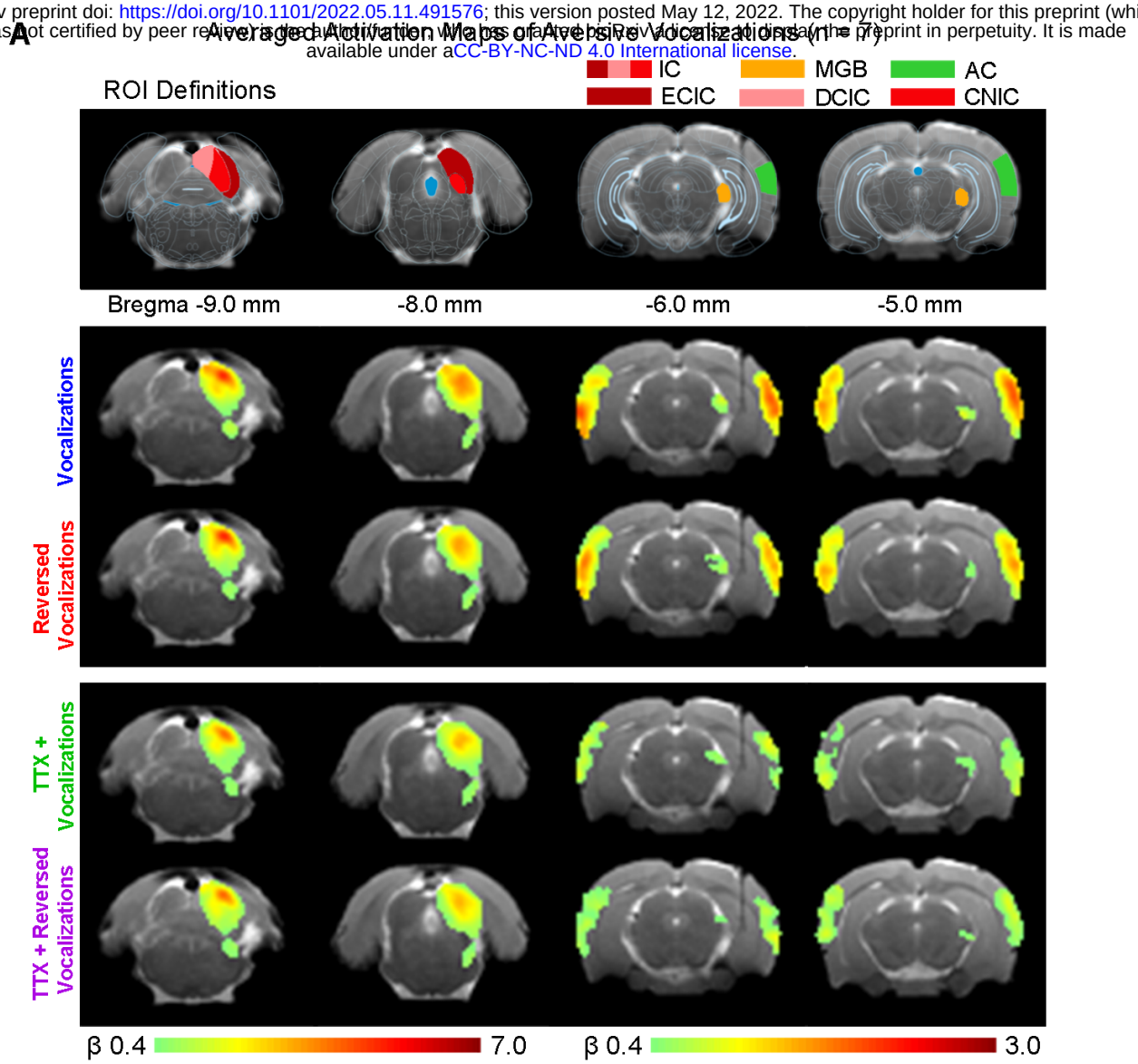

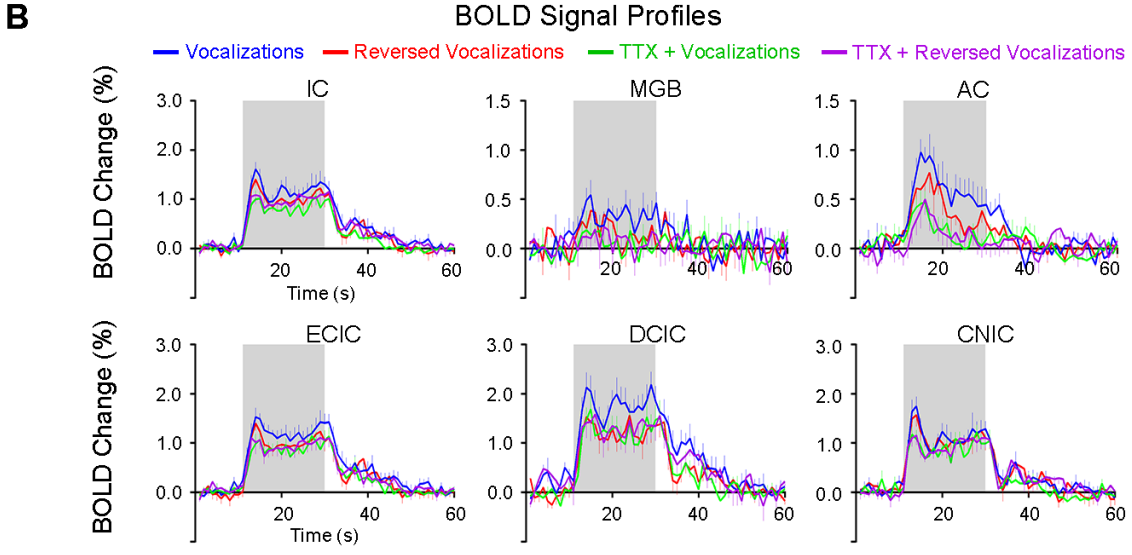

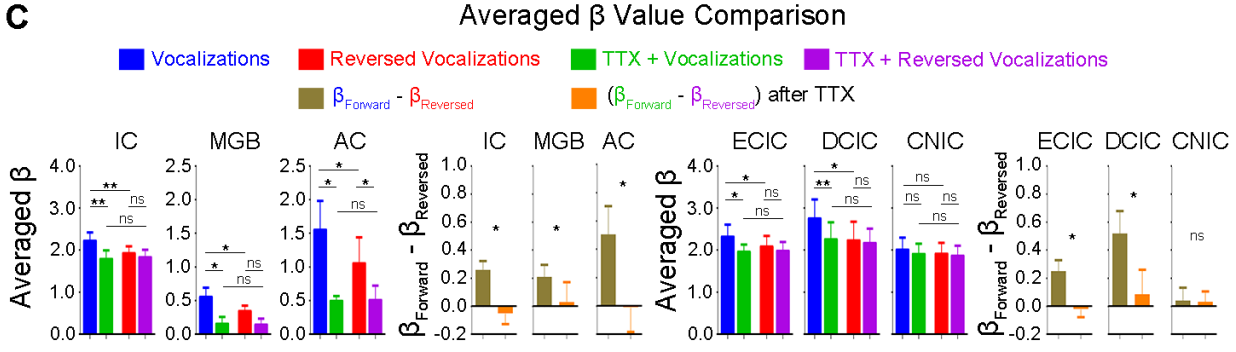

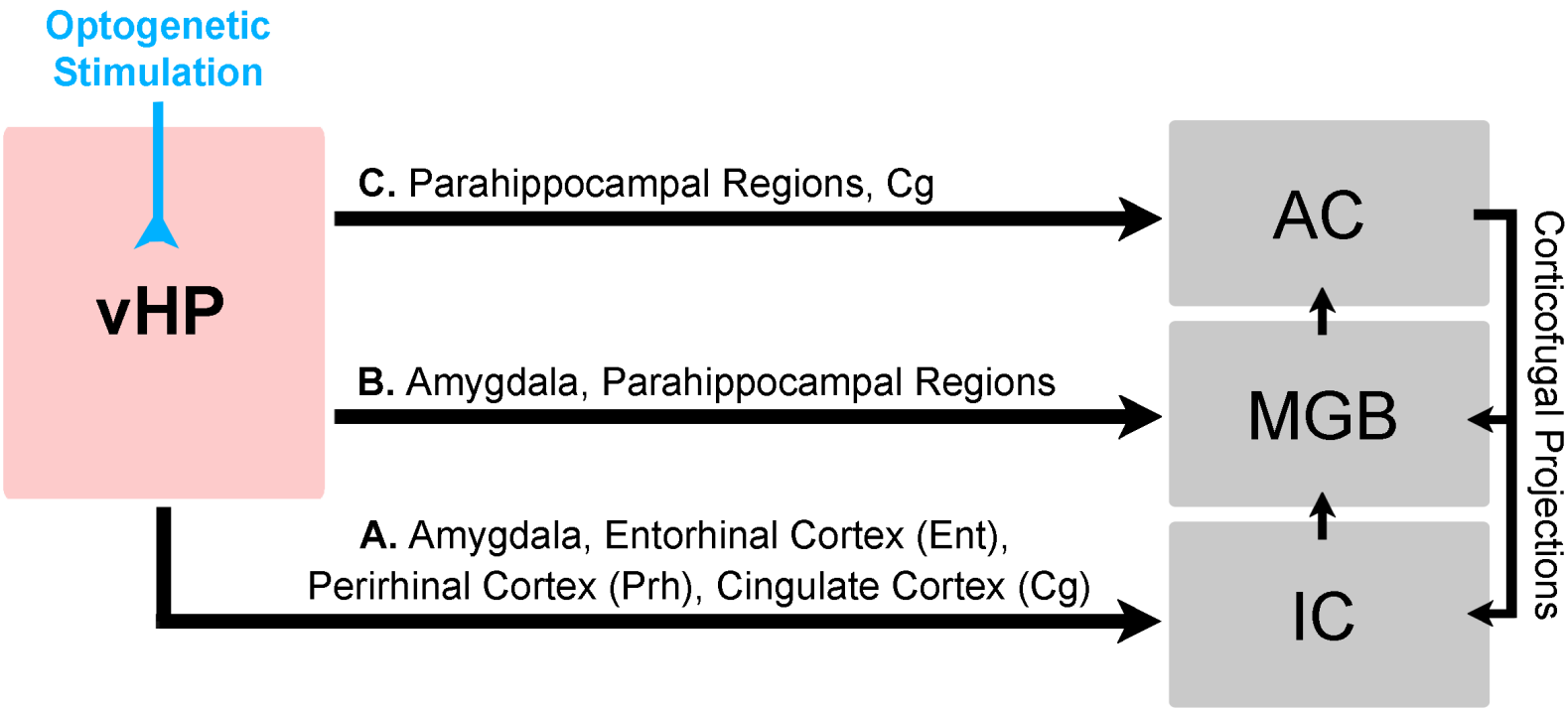

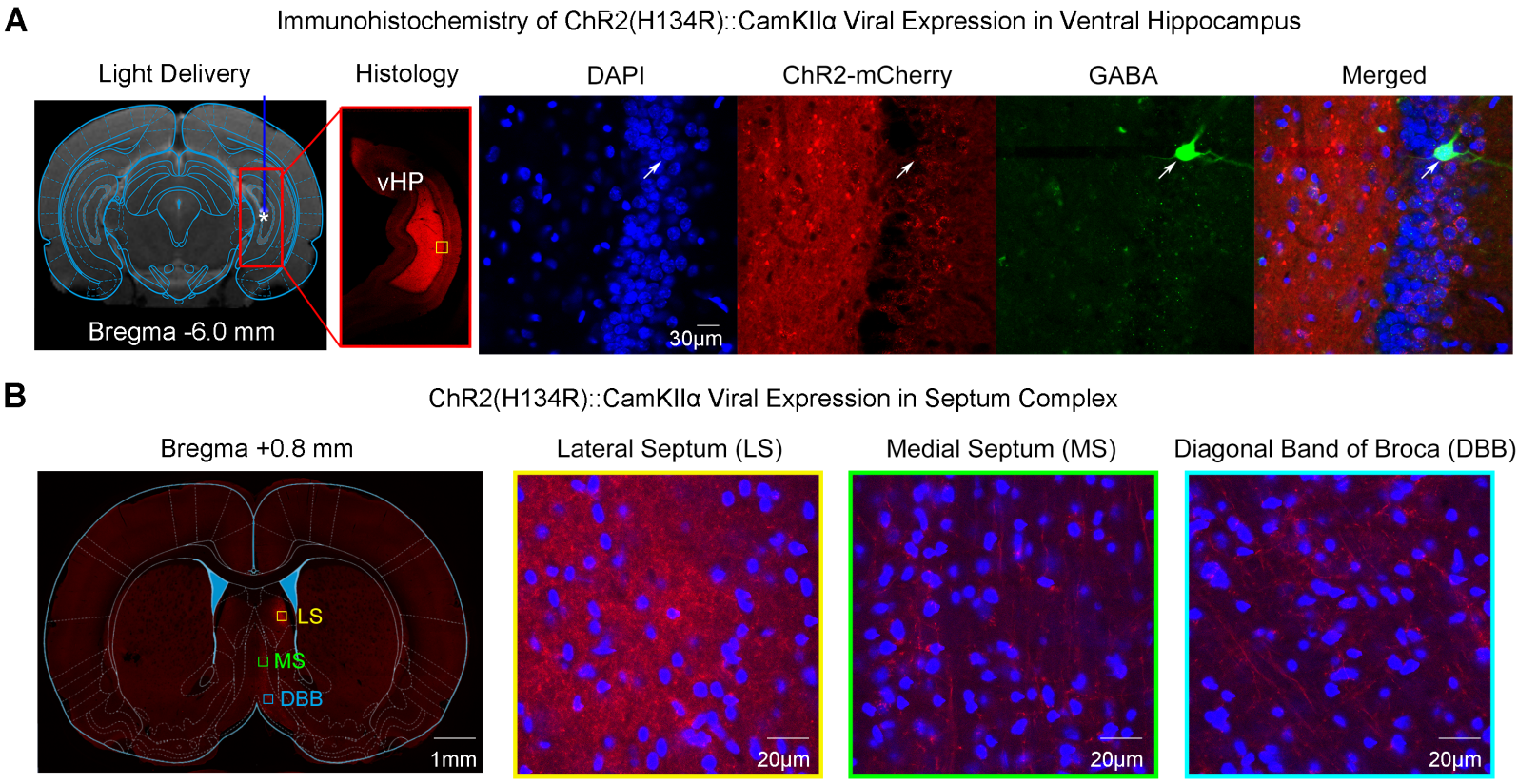

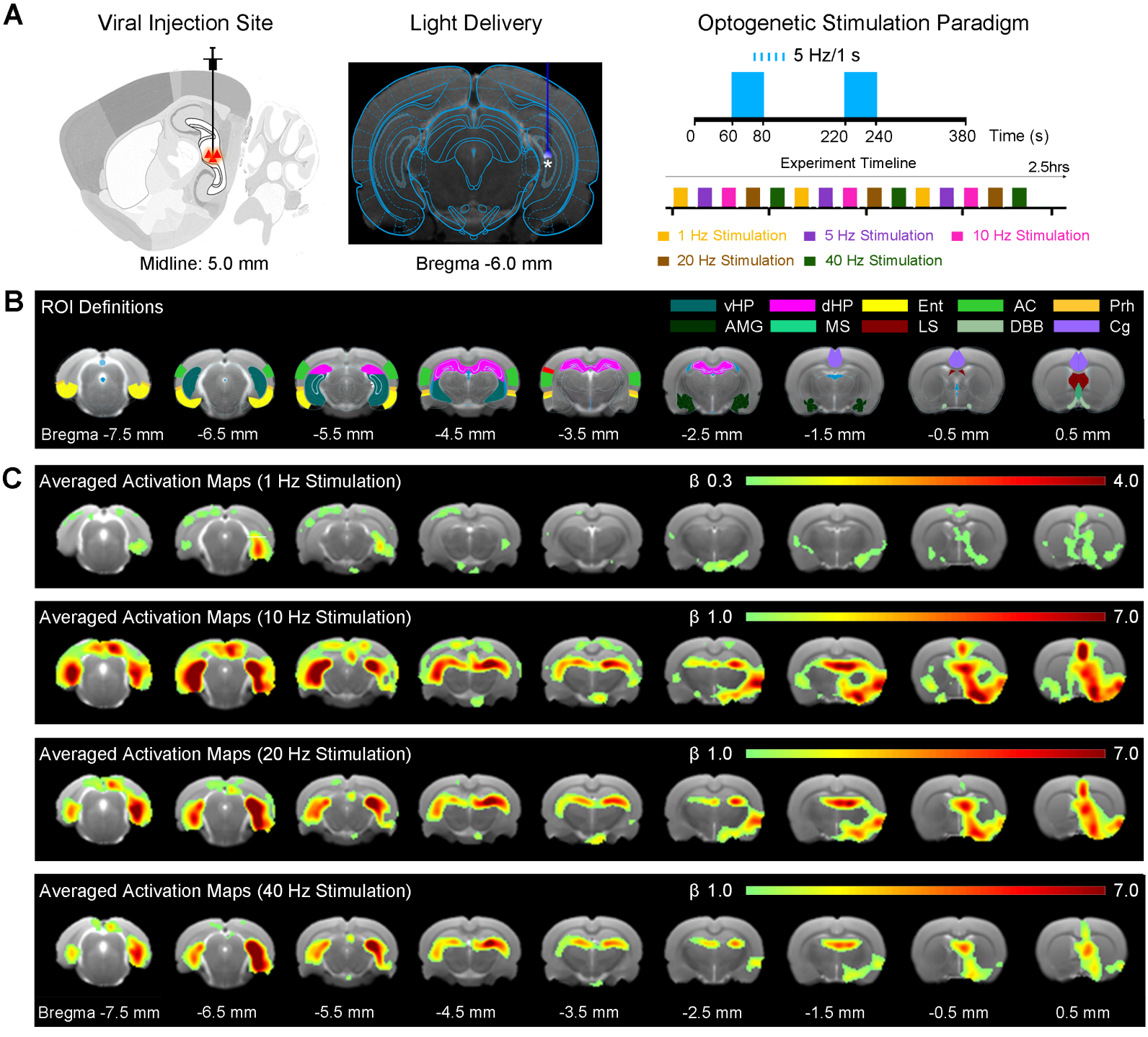

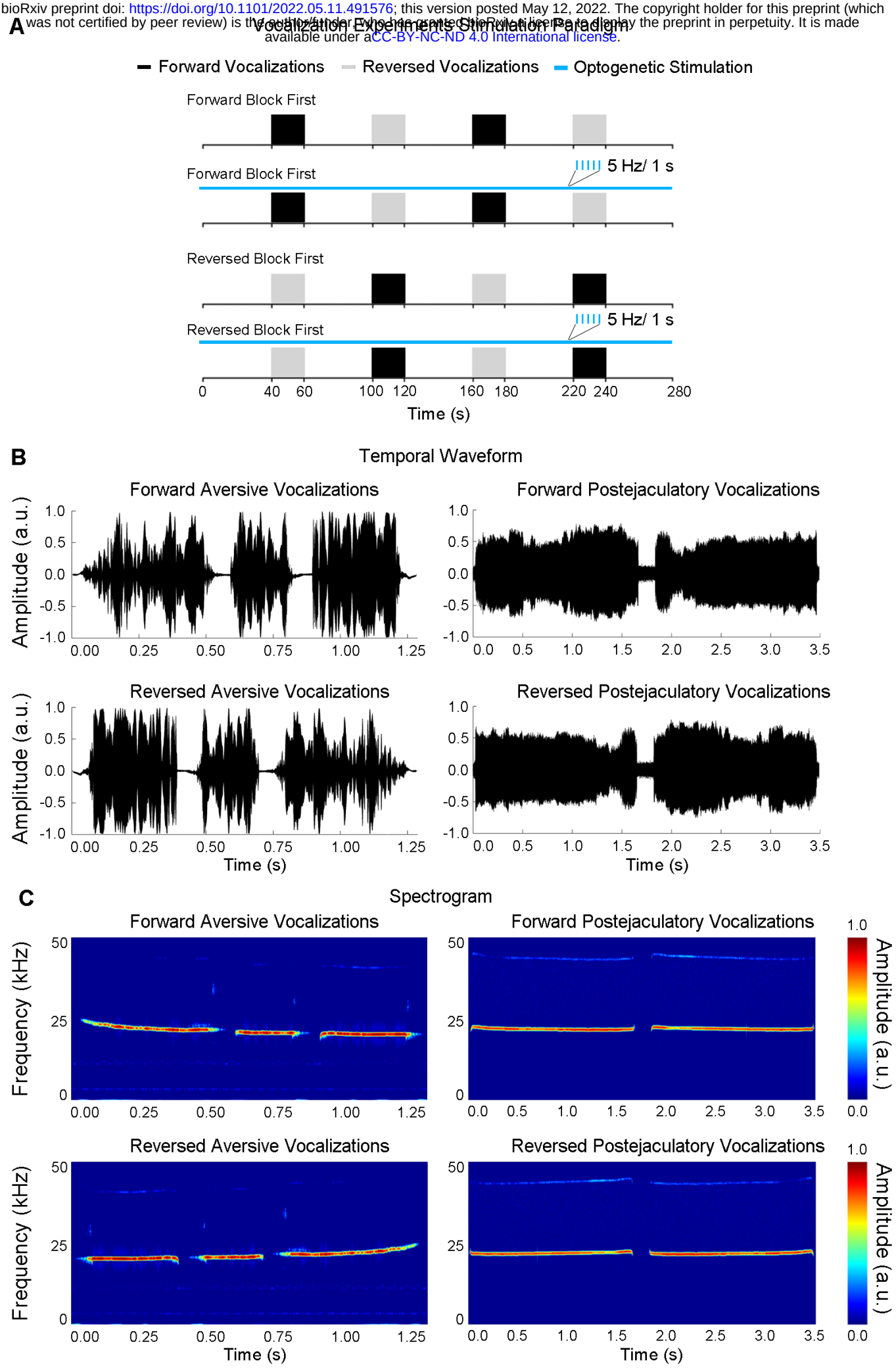

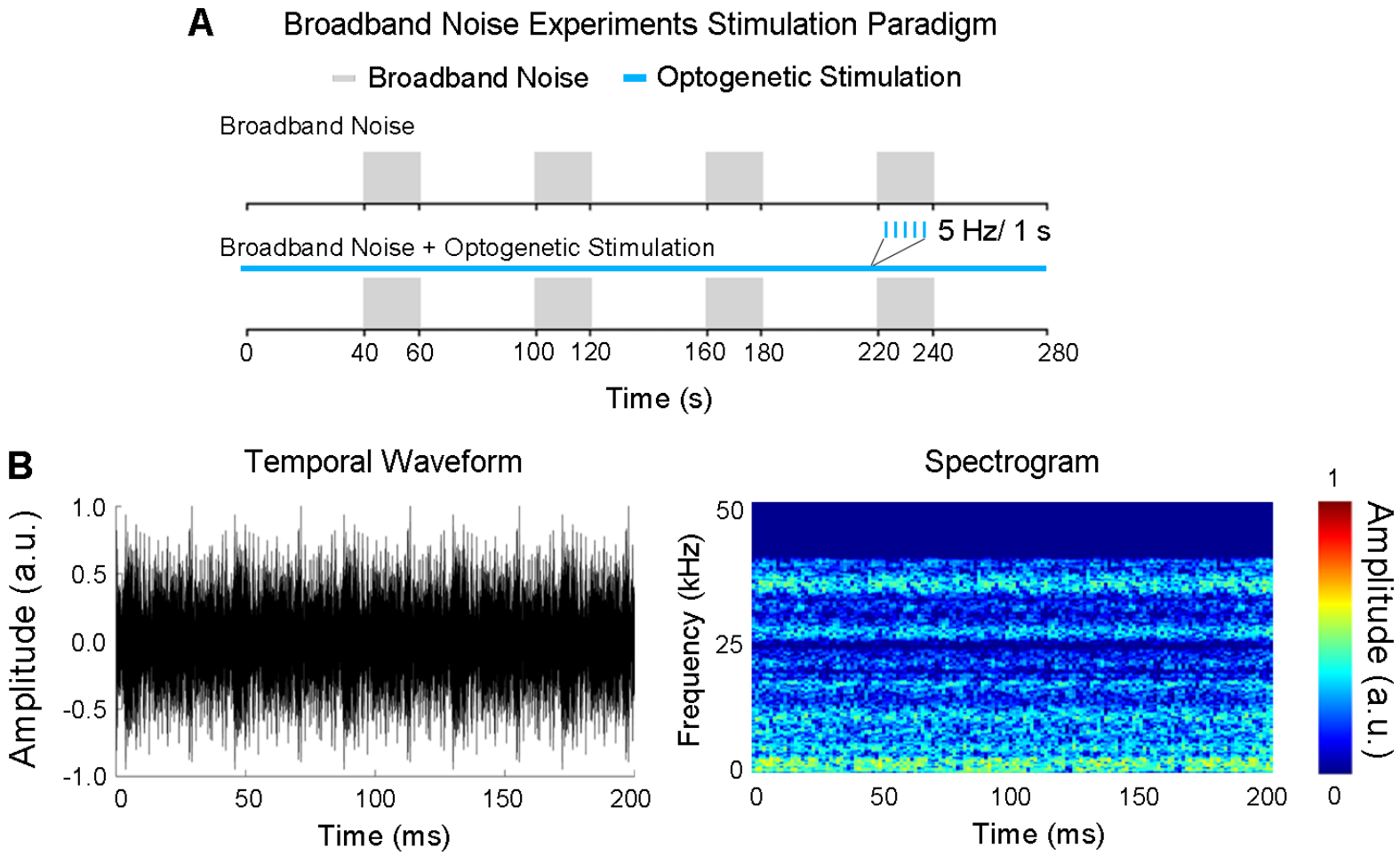

A

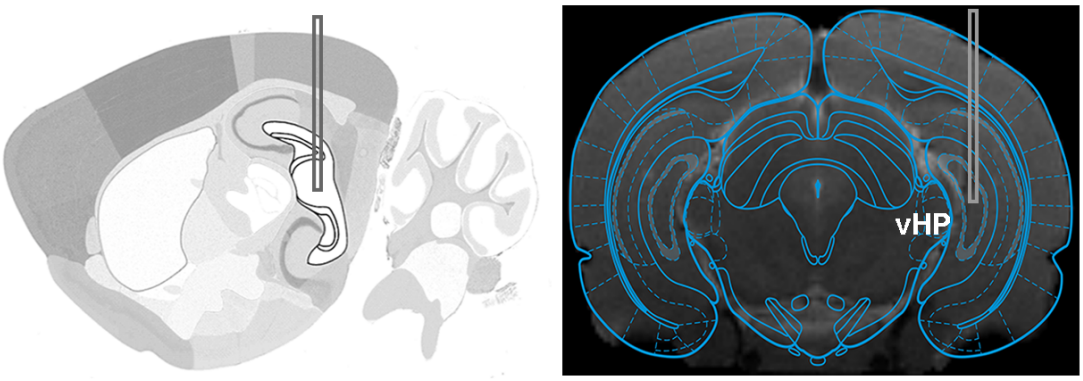

B

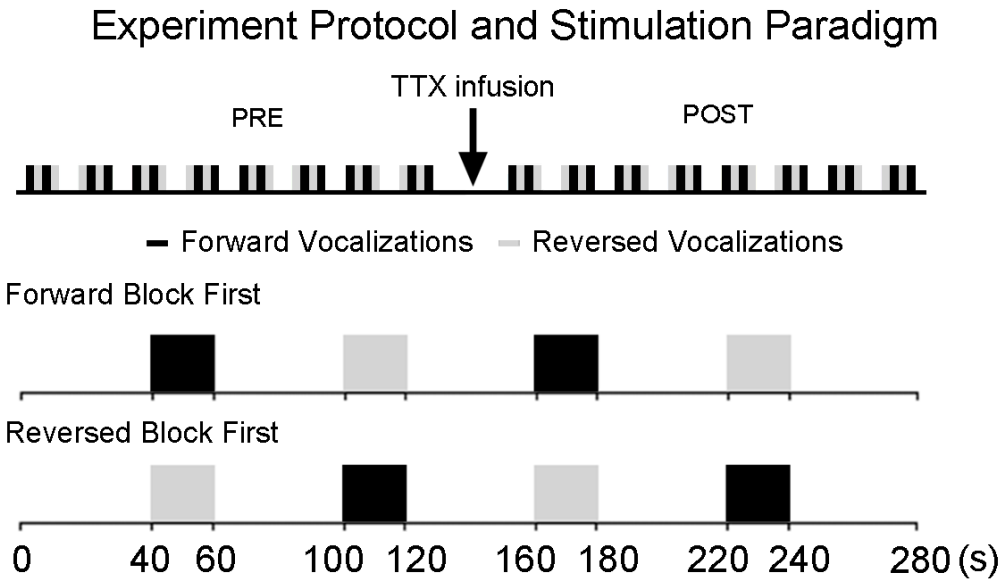

C

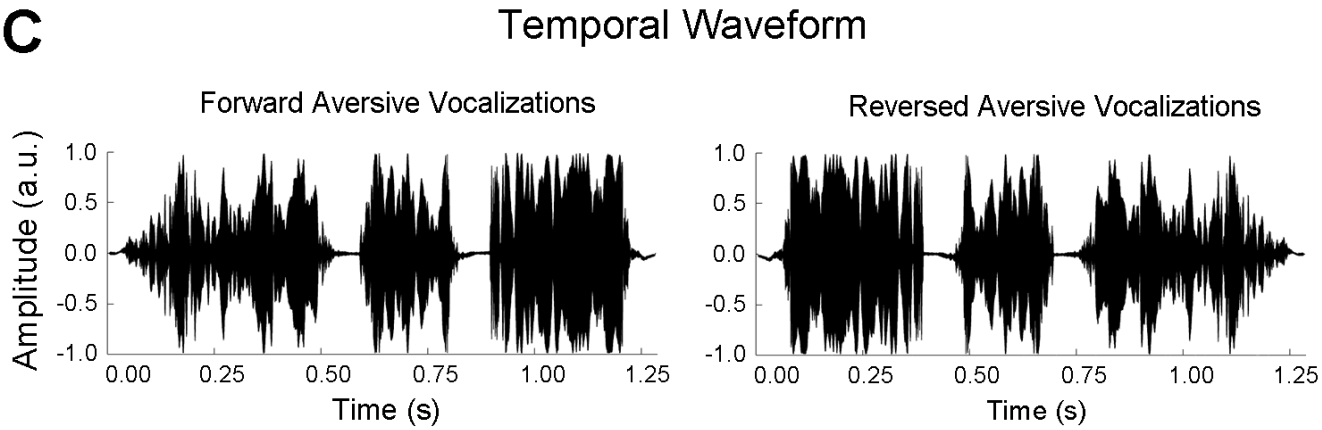

D